Thermal studies on the lower Carboniferous basins of Khenifra and Qasbat-Tadla, Morocco: What do they teach us about the pre-Variscan stages in NW Africa?

R. Lepretre, Mohamed El Houicha, Andrea Schito, Rachid Ouchaou, Francis Chopin, Pedro Cózar

Journal of African Earth Sciences 219 (2024) 105406

Contents lists available at ScienceDirect

Journal of African Earth Sciences

journal homepage: www.elsevier.com/locate/jafrearsci

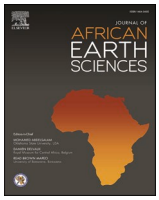

Thermal studies on the lower Carboniferous basins of Khenifra and Qasbat-Tadla, Morocco: What do they teach us about the pre-Variscan stages in NW Africa?

R. Leprêtre [a,*], M. El Houicha [b], A. Schito [c,d], R. Ouchaou [e], F. Chopin [f,g], P. Cózar [h]

[a] GEC, CY Cergy Paris Université, France
[b] Faculté des Sciences (LGG), Université Chouaib Doukkali, El Jadida, Morocco
[c] Departament of Mineralogy, Petrology and Applied Geophysics, Faculty of Earth Sciences, University of Barcelona, UK
[d] Department of Geology and Petroleum Geology, School of Geosciences, University of Aberdeen, Aberdeen, AB24 3UE, UK
[e] LOG UMR 8187, Université de Lille, Lille, France
[f] EOST, IPGR, UMR7516, Université de Strasbourg, France
[g] Center for lithospheric Research, Czech Geological Survey, Praga, Czech Republic
[h] Instituto de Geociencias CSIC-UCM, Madrid, Spain

ARTICLE INFO

Handling Editor: M Mapeo

Original content: Khenifra_Raman-all-spectra (Original data)

ABSTRACT

Within the Variscan Belt of Morocco, the Central Massif preserves Early Carboniferous rift basins. The Lower Carboniferous Khenifra and Qasbat-Tadla basins are aborted rifts, developed just before the Variscan orogenesis in Morocco that occurred during the Pennsylvanian-Cisuralian in NW Africa. Due to both weak inversion of these basins during the Variscan orogeny and limited burial afterwards, these basins offer the opportunity to study the Early Carboniferous pre-orogenic thermal regimes. In the Khenifra basin, 77 samples collected across the basin and its basement's boundaries, allowed the determination of the maximal temperature reached during the rocks burial by means of Raman spectroscopic analyses. The Ordovician basement shows mean temperatures between 230 and 300 °C whereas the upper Visean/Serpukhovian infill has a wide range, from temperatures <160 °C to 250–260 °C. This thermal variation within the basinal series has been evidenced from west to east and cannot have been acquired during the Variscan events. The acquisition of these maximal temperatures occurred between Late Devonian to Upper Visean/Serpukhovian and is thought to result from the formation of an extended rift. In the Qasbat-Tadla basin, Rock-Eval data from Ordovician to Devonian source-rocks indicate significantly lower maximal temperatures reached by pre-Carboniferous samples that are within the oil window. Our results are in favor of a heterodox model for the Variscan belt in Morocco and NW African in general, suggesting that no pre-Variscan compressional events are needed. Instead, the development of the intraplate Variscan belt in NW Africa was permitted through the development of hot and weak Lower Carboniferous basins, subsequently inverted in a far-field stress field. The striking thermal differences between the Khenifra and Qasbat-Tadla basins suggest that important tectonic segmentation must have shaped the area during the Early Carboniferous extensional phase.

1. Introduction

The portion of Variscan belt preserved in NW Africa is consensually considered an intraplate segment (Hoepffner et al., 2005, 2006; Michard et al., 2008, 2010; Leprêtre et al., 2024). No oceanic suture is recorded, and if any, it is probably obscured by the Atlantic nowadays. With this in mind, the NW African Variscides appear distal compared to the "suture" and the main orogenic wedge and they are indeed not organized at all as an orogenic prism. In this case, what kind of crustal inheritance or mechanisms must be looked for to explain the development of this distal intraplate deformation during the main compression stage of Late Pennsylvanian-Cisuralian times? This question was solved by previous authors by suggesting that a subduction (with various hypotheses regarding the location of subduction front and its vergence) was controlling the intraplate deformation far from the subduction front in the Meseta domain (Roddaz et al., 2002; Accotto et al., 2020; Michard et al.,

* Corresponding author.
E-mail addresses: remi.lep@gmail.com, remi.lepretre@cyu.fr (R. Leprêtre).

https://doi.org/10.1016/j.jafrearsci.2024.105406
Received 30 May 2024; Received in revised form 26 August 2024; Accepted 28 August 2024
Available online 1 September 2024

2010, 2023). In this view thus, the subduction – as the first-order mechanism – enabled early tectonics with the development of a wide lower Carboniferous basin system throughout N. Morocco and NW Algeria. It was associated with magmatism, but also with a tectono-metamorphic compression phase, namely the Eovariscan phase.

The southern Azrou-Khenifra basin (AKB; Figs. 1 and 2) offers the opportunity to study a key area in the evolution of the NW African Variscan belt. Indeed, it is one of the main Lower Carboniferous basins that crop out in Morocco (Fig. 2). Yet, a debate is still open regarding the tectonic conditions during its development. It is generally considered that this basin developed, after a contractional Eovariscan phase that took place between Late Devonian to Tournaisian (Piqué and Michard, 1989), in a strike-slip or extensional context (Huvelin, 1973; Allary et al., 1976; Beauchamp and Izart, 1987; Bouabdelli, 1989; El Houicha, 1994). Some authors considered a fully contractional setting for its development, since the Tournaisian or Early Visean (Ben Abbou, 2001; Ntarmouchant, 2003; Michard et al., 2010, 2023; Lahfid et al., 2019), whereas other authors considered an extensional development for the Late Visean-Serpukhovian main infill (*e.g.* Vachard et al., 2006) or even since the Late Devonian, as a continuum up to the Serpukhovian at least (Leprêtre et al., 2024). Since this basin suffered limited inversion during the Variscan stages, it could theoretically allow accessing the pre-Variscan thermal conditions. In a recent study, Lahfid et al. (2019) used Raman spectroscopy and already considered this issue, but mainly from a « basement » point of view, since they mostly sampled the Ordovician basement of the Zaian massif, which represents the western shoulder of the Khenifra basin (Fig. 2). These authors evidenced unexpected high basement temperatures and correlated them to a Late Devonian high temperature event could have been responsible for paleogeotherms as high as 60 °C.km^{-1} within the Zaian basement. Lying directly south of the southern AKB, below a flat Mesozoic-Cenozoic cover, the Lower Carboniferous Qasbat-Tadla basin (Fig. 2) has also been the object of several works since a long time (Jabour and Nakayama, 1988; Verset, 1985, 1988; Er-Raïoui et al., 2001), based on the study of subsurface data (wells and seismic data) and organic matter geochemistry.

Regarding the long-lasting debate on the pre-orogenic stages of the Variscan story in NW Africa (Leprêtre et al., 2024), we focused our study on two Lower Carboniferous basins in order to document their thermal evolution during the Late Paleozoic. The thermal record will be used as a fingerprint in order to assign these basins to a specific tectonic evolution. The first studied area is the Khenifra basin. Here, we have sampled 77 rocks mainly from the basinal Visean-Serpukhovian series (Cózar et al., 2023a), but also from the Ordovician basement in order to determine their maximum temperatures relying on the Raman Spectroscopy of Carbonaceous Matter (RSCM). This method was first developed by Beyssac et al. (2002) and Lahfid et al. (2010). With some recent developments (*e.g.* Lünsdorf et al., 2017), it is able to determine maximum temperature reached by the rocks in the course of their history, from 150/160 °C–650 °C. We also used organic matter

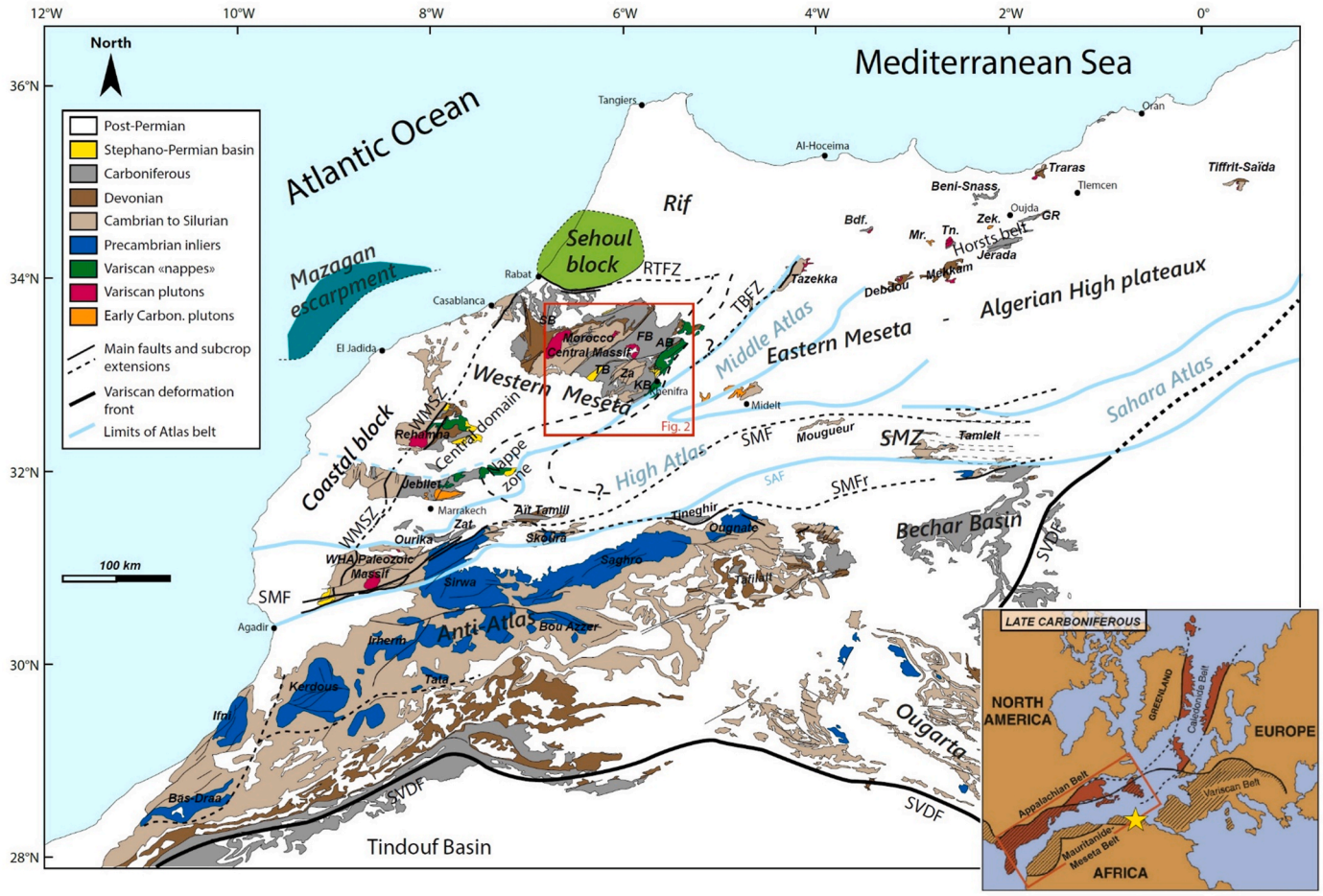

Fig. 1. Geological map of North Morocco (after Hollard et al., 1985; Michard et al., 2010). Ages information for plutonic bodies comes from (Chopin et al., 2023 and references therein). ***Faults:*** RTFZ: Rabat-Tiflet Fault Zone; SMFZ: South Meseta Fault Zone; SMFr: South Meseta Front; SVDF: South Variscan Deformation Front; TBFZ: Tazekka-Bsabbis Fault Zone. ***Areas & zones:*** AB: Azrou Basin; Bdf: Boudoufoud; FB: Fourhal Basin; GR: Ghar Roubane; KB: Khenifra sub-basin; Mr: Merguechoum; SB: Sidi Bettache Basin; SMZ: South Meseta Zone; Tn: Tanncherfi; TB: Telt Basin; WHA: Western High Atlas; Za: Zaian; Zek: Zekkara. On the bottom right, a sketch shows the general paleogeographical configuration at the end of the Late Carboniferous, with position of Morocco (yellow star).

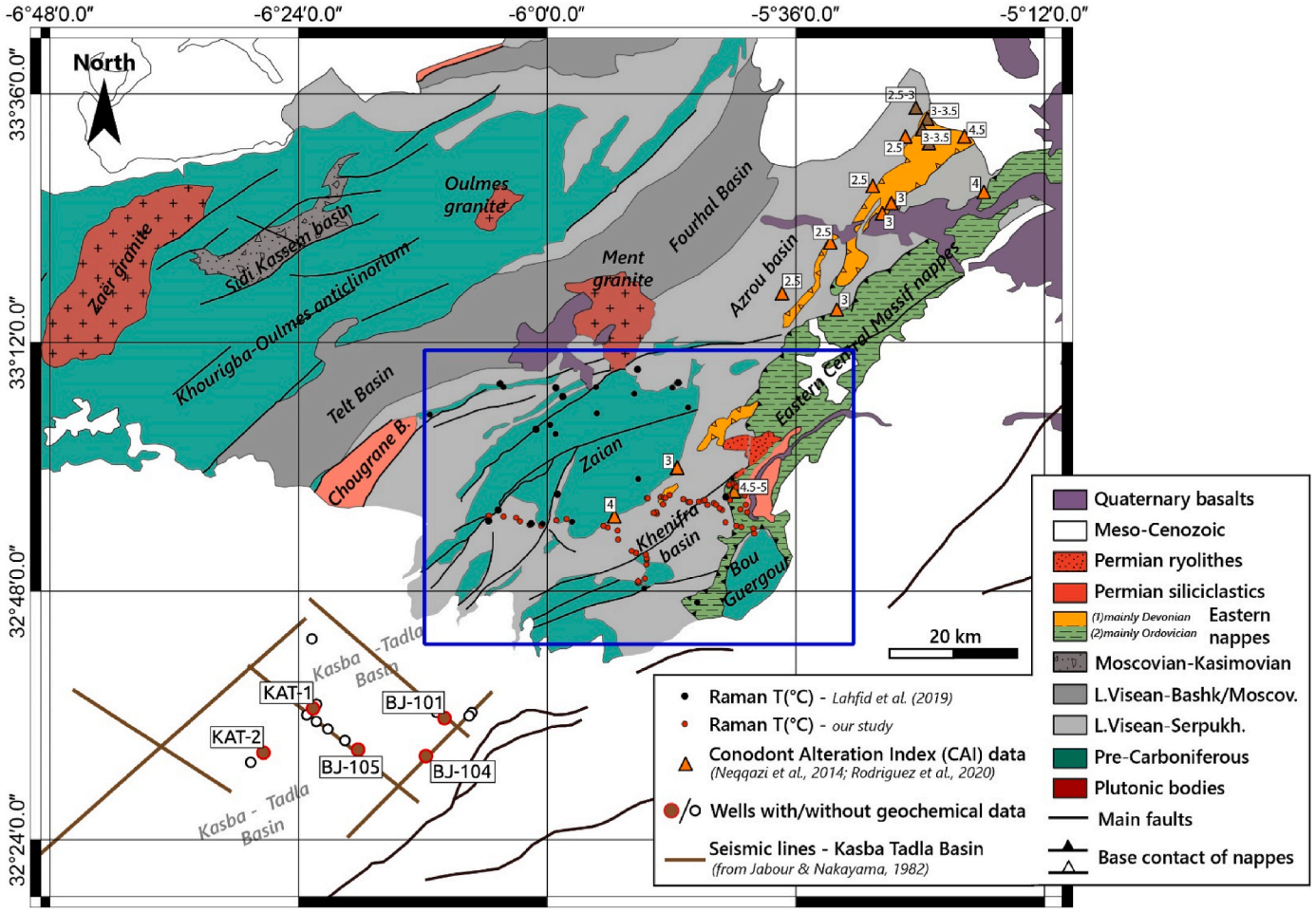

Fig. 2. Structural map of the eastern Central Massif (modified after Verset, 1985), with location of the geological map of the Khenifra sub-basin and its boundaries (blue rectangle; Fig. 3). Within the Khenifra sub-basin, black and red dots are showing Lahfid et al. (2019) and our samples locations, respectively. Orange triangles represent thermometry results using the Conodont Alteration Index (from Neqqazi et al., 2014; Rodríguez et al., 2020). South of the Zaian, brown lines indicate the traces of seismic lines used in Jabour and Nakayama (1988) in the Qasbat-Tadla basin. All the wells positions are from Verset et al. (1988). In red, it indicates the wells where geochemical datasets are available.

geochemical data from the Qasbat-Tadla basin which is located directly southward of the Khenifra basin (Figs. 1 and 2). By using these two different datasets, we propose a new tectonic evolution of these basins during the Late Paleozoic and reconsider their importance in the development of the Variscan stages in NW Africa.

2. Geological setting

2.1. Main elements of the NW African Variscides (Fig. 1)

The Variscan belt in Morocco represents the southern extension of the Variscan belt of Western Europe. It is considered as an intraplate belt (*e.g.* Hoepffner et al., 2005; Michard et al., 2010; Leprêtre et al., 2024), developed in front of the main orogen whose fold-and-thrust belt is still well-preserved along the east American margin in the Appalachian (*e.g.* Hatcher et al., 2010). Compared to the West European segments of the Variscan belt, the NW African Variscides happen to undergo their major deformation later, from the Pennsylvanian until the Cisuralian (among others: Hoepffner et al., 2005; Simancas et al., 2009; Hatcher et al., 2010; Michard et al., 2010; Ballèvre et al., 2014; Franke et al., 2017; Edel et al., 2018). In details, the NW African Variscides are classically divided into different tectono-sedimentary domains (*e.g.* Leprêtre et al., 2024, Fig. 1). **South of the South Meseta Zone (or Sub-Meseta Zone; SMZ), the Anti-Atlas domain** represents a thick-skinned Variscan fold-and-thrust belt, inverting the northern boundary of the West African Craton (Burkhard et al., 2006; Baidder et al., 2016). **North of the SMZ, the Meseta domain** is generally subdivided between the Western and Eastern Meseta. This is the result of the Meso-Cenozoic evolution of the inverted Middle Atlas rift, re-using a former Paleozoic fault zone, the Tazekka-Bsabis-Bekrit Fault Zone (TBBFZ; Morin, 1973; Hoepffner et al., 1978; Charrière, 1990; Bouabdelli and Piqué, 1996). The Western Meseta encompasses the most deformed Variscan domains. It shows widespread pre- and syn-Variscan magmatism and the local development of Barrovian metamorphism (*Magmatism evidences:* Mrini et al., 1992; Kharbouch, 1994; El Hadi et al., 2006; Delchini et al., 2018; Chopin et al., 2023; *deformations & metamorphism in the Rehamna & Jebilet massifs:* Chopin et al., 2014; Wernert et al., 2016; Delchini et al., 2018 and references therein). Aside to these very deformed Variscan domains, the Western Meseta also contains Devonian-Carboniferous basins, whose best example is the Sidi Bettache (SB) in the Morocco Central Massif (MCM; Fig. 1). East of the TBBFZ, the Eastern Meseta is less deformed during the upper Pennsylvanian/Cisuralian Variscan events (Er-Raji, 1997; Hoepffner, 1987; Michard et al., 2010). Yet, it has been characterized by a widespread "Eovariscan" deformation event, occurring somewhere between Late Devonian and Early Visean, following the different authors (Hoepffner, 1987; Torbi, 1996; Accotto et al., 2020). This deformation also exists to the SE the MCM in Western Meseta (Hoepffner, 1987; Allary et al., 1976; Bouabdelli, 1989). Its origin remains debated, between extensional explanations, contractional or a subtle combination of both (*extensional*: Leprêtre et al., 2024;

Houari, 2003; Diot and Bouchez, 1989; *compressional*: Hoepffner, 1987; Accotto et al., 2020; *mixture of both*: Bouabdelli and Piqué, 1996; Lahfid et al., 2019, Michard et al., 2022). Subsequently, the upper Pennsylvanian-Cisuralian Variscan events also affected the Eastern Meseta. **The SMZ** is a transitional zone between the Meseta and the Anti-Atlas domains showing mainly transpressive deformation (Houari and Hoepffner, 2003; Michard et al., 2010). At last, the Sehoul block in the north is a crustal block whose origin (Meseta? Avalonia? Meguma? See discussions in Michard et al., 2010, 2023; Tahiri et al., 2010; Chopin et al., 2014) and timing of accretion against the Meseta (Early or Late Carboniferous? See discussions in Letsch et al., 2018; Michard et al., 2023; Leprêtre et al., 2024) remain debated.

2.2. The Khenifra-Zaian area within the MCM

The Khenifra and Qasbat-Tadla (or Kasba-Tadla) sub-basins belong to both the Central zone and the Nappes zone of the Western Meseta (Fig. 1). The Central Zone is structured in alternating basins and highs (Figs. 1 and 2): the troughs generally preserved Devonian-Carboniferous inverted basins whereas the highs usually show penetrative deformations associated to low-grade greenschist facies (see review by Michard et al., 2008). Locally, Barrovian metamorphism has been recognized in the Rehamna and Jebilet inliers (*for the Rehamna:* Hoepffner, 1974; Michard, 1982; Corsini et al., 1988; Chopin et al., 2014; Wernert et al., 2016; *for the Jebilet:* Huvelin, 1977; Delchini et al., 2018). The Nappes Zone fringes the Khenifra and Qasbat-Tadla basins to the east, with west-verging allochthonous units visible outcropping to the east of the Khenifra basin and mainly constituted from Upper Ordovician material (Fig. 2; Allary et al., 1976; Bouabdelli, 1989, 1994).

Let us notice here that in general the expression "Khenifra basin" is used to talk about the southern half of the more extended AKB. By doing so, the "Khenifra basin" corresponds to a geographical unit that is not obviously a geological one. The "Khenifra basin" can be subdivided in turn into the Sidi Lamine and Khenifra sub-basins (Fig. 3), each of them showing different stratigraphical terms. In the following, when the precision is not needed, the "Khenifra basin" will represent both Sidi Lamine and Khenifra sub-basins and we will specify which one of the two sub-basins if needed.

2.2.1. General stratigraphy

The Khenifra basin is sandwiched between the Zaian structural high to the west and the Nappes zone to the east, that are directly bounded by the Middle Atlas (Figs. 1–3). This basin and the Qasbat-Tadla one to the south, below the Ceno-Mesozoic Phosphates plateau, have been the focus of structural and stratigraphical works (Allary et al., 1976; Huvelin, 1973; Izart, 1990; Huvelin and Mamet, 1997; Jabour and Nakayama, 1988; Verset et al., 1988; Bouabdelli, 1989; El Houicha, 1994; Bouabdelli and Piqué, 1996; Er-Raïoui et al., 2001; Lahfid et al., 2019). In the following description, we will call "basement" those rocks represented by (1) the stratigraphical formations older than the Early-Late Visean and (2) that have undergone a metamorphic deformation event, namely the "Eovariscan" event (*i.e.* mostly Precambrian to Ordovician rocks; Figs. 2 and 3).

The autochthonous basement largely crops out in the Zaian massif, to the west and north of the area, in the NE-SW oriented Jbel Hadid and Bou Acila small highs in the south and to the SE, and also within the Bou Guergour massif (Fig. 3), which is a tectonic window overlain by the upper Ordovician Khenifra nappe (Allary et al., 1972). Within these basement massifs, stratigraphical sections span Precambrian (Ediacaran) to upper Ordovician sediments (Drot and Morin, 1962; Allary et al., 1976; Verset et al., 1988; Badra and Cailleux, 1983; Bouabdelli, 1989; Ouabid et al., 2017, 2023; Letsch et al., 2018; El Houicha et al., 2018). On top of the lower(?)-middle Ordovician alternations of quartzitic bars and micaceous-sandy pelites (Fig. 4A), well-dated Upper Ordovician formations, called "Asfar schists", are instead showing alternations of sandstones and pelites, estimated to reach no more than 800 m of thickness (Badra and Cailleux, 1983; Bouabdelli, 1989; Verset et al., 1988); topped by quartzitic levels with glaciogenic deposits (El

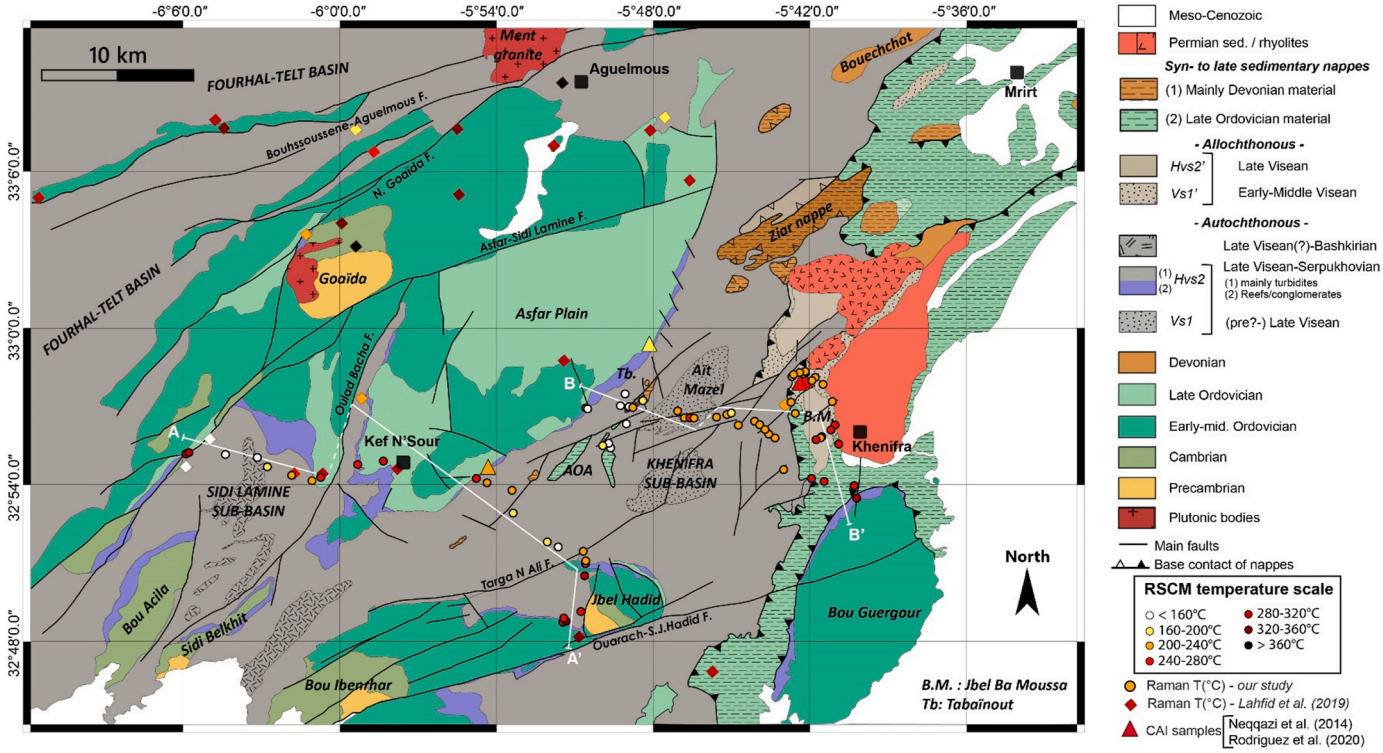

Fig. 3. Geological map of the Khenifra basin and surroundings Ordovician basement massifs [modified after Verset et al. (1988), Bouabdelli (1989); El Houicha (1994); Lahfid et al. (2019); Rodríguez et al. (2020), and M. El Houicha personal observations].Circles and diamonds show our samples and Lahfid et al. (2019) ones, respectively. Color scale is similar for both datasets and indicated on the map. AOA: Aït Ou Azzouz; BM: Ba Moussa; Tb: Tabaïnout.

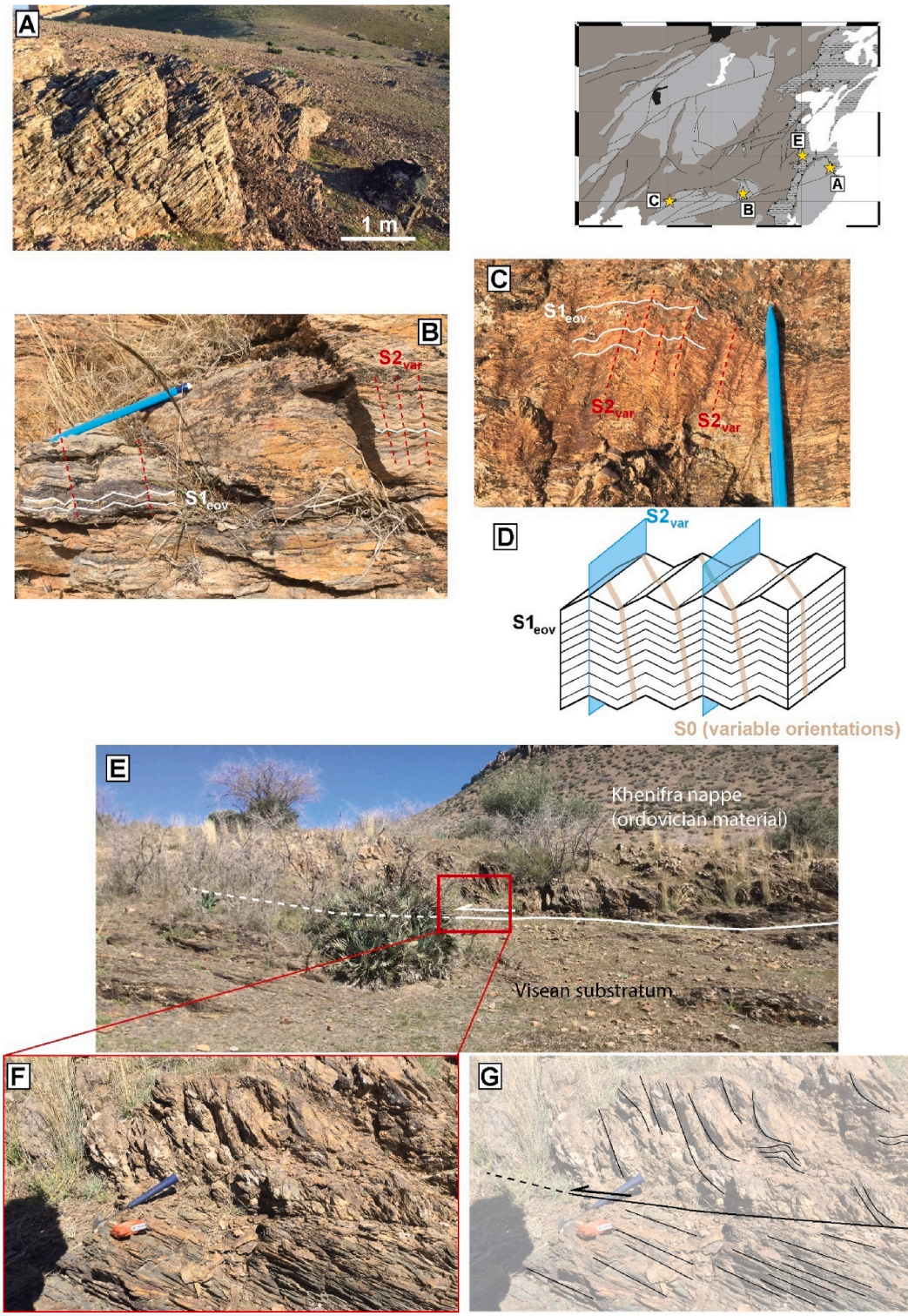

Fig. 4. Photographic plate showing the basement formations and their deformation by the Eovariscan event. Locations on small grey-shaded map. (A) Tilted schistosed fine sandstones in Bou Guergour. (B) Crenulated $S1_{eov}$ (Eovariscan) cleavage in Precambrian(?)-Cambrian of Jbel Hadid. (C) Similar deformation in Cambrian gneiss in Bou Ibenrhar. (D) Schematic relationships between bedding S0 and cleavages $S1_{eov}$ and S2 (Variscan). (E) View of the contact between Khenifra nappe and underlying upper Visean basinal formations. (F, G) Zoom on the basal contact of the Khenifra nappe.

Houicha M. & Ghienne J.-F.personal observations). Very similar lithologies are recorded within the Khenifra nappe for the Late Ordovician (Bouabdelli, 1989; El Houicha, 1994, Fig. 4F). The Zaian massif is devoid of Silurian and Devonian rocks. The Silurian can only be found in small outcrops, north of the Zaian massif, (Silurian of Tichount n'Rich, Bouechchot andin Mrirt nappe in Faik [1988]). It is represented by a *ca.* 100m-thick formation of the classical graptolitic black shales (review in Bouabdelli, 1989; *for sub-surface in Qasbat-Tadla*: Verset et al., 1988). After the Early Paleozoic, mainly marine influences were recorded from the Middle/Late Devonian to the end of Early Carboniferous. Within the upper Visean-Serpukhovian infill, the famous Bouechchot outcrop shows the only autochthonous cropping out Devonian coexisting with

allochthonous Devonian klippen, olistostromes or clasts, whose sources could likely be the Ziar-Mrirt nappes (Sidi Ammar, Bou Imezdaoun; see Faïk, 1988; El Houicha, 1994). Indeed, Devonian outcrops are well-represented within the Ziar-Mrirt nappe (Ziar, Anajdam, Touchchent-Akellal, Gara de Mrirt; see Allary et al., 1976, Bouabdelli, 1989; Faïk, 1988; Becker et al., 2020).The Qasbat-Tadla wells pierced through supposedly autochthonous Devonian series from the Famennian (KAT-2 well) or the Early Devonian (BJ-101, BJ-104 wells) mainly composed of black shales.

The main infill of the basin occurred during the Late Visean up to the Serpukhovian (see recent stratigraphic revisions in Cózar et al., 2020, 2023a). Synthetic columns showing the distribution of stratigraphical ages across the Khenifra basin are given in Fig. 5, mainly based on El Houicha (1994) and revised by Rodríguez et al. (2020) and Cózar et al. (2020, 2023a). When cropping out, the oldest unconformable deposits on top of the autochthonous basement are upper Visean in age (Tabaïnout, Jbel Hadid; Fig. 5) immediately followed upward by Serpukhovian rocks (Hvs2, see Fig. 5; Cózar et al., 2023a). Upper Visean rocks also likely crop out within the Aït Mazel antiform (Hvs1, Figs. 3 and 5; El Houicha, 1994) whereas outcropping rocks in the rest of the basin can largely be considered Serpukhovian in age (Cózar et al., 2023a). By contrast, on the allochthonous Khenifra nappe eastward of the basin, unconformable deposits on top of Ordovician schists, likely recorded the full Visean stage (Early(?)-Middle Visean: Vs1'; Late Visean: Hvs2'; Fig. 5), without proved Serpukhovian ages (Bouabdelli, 1989; El Houicha, 1994; Huvelin and Mamet, 1997; Rodríguez et al., 2020; Cózar et al., 2020).

On the allochthonous Khenifra nappe, in the Ba Moussa syncline, Vs1′ deposits show lenticular breccia, sandstones (calcareous ?) followed upward by sandy/pelitic levels and siltstones, with an intervening wildflysch level (Fig. 5). Upward, Hvs2′ deposits are unconformably either on top of Vs1′ or directly on the upper Ordovician rocks (Fig. 3). Hvs2' deposits show a basal breccia directly followed by sandy and calcarenitic bioclastic limestones. Thick fine siliciclastic (sandstones/siltestone) series follow upward, with only some biodetrital calcarenites occurrences close to its base in the Ba Moussa syncline.

On top of the Precambrian-Ordovician basement, close to the boundaries of the Khenifra basin, the basal member of the upper Visean-Serpukhovian series (Hvs2), that can reach tens of meters, shows transgressive deposits with carbonates (exemplified in the Tabaïnout:

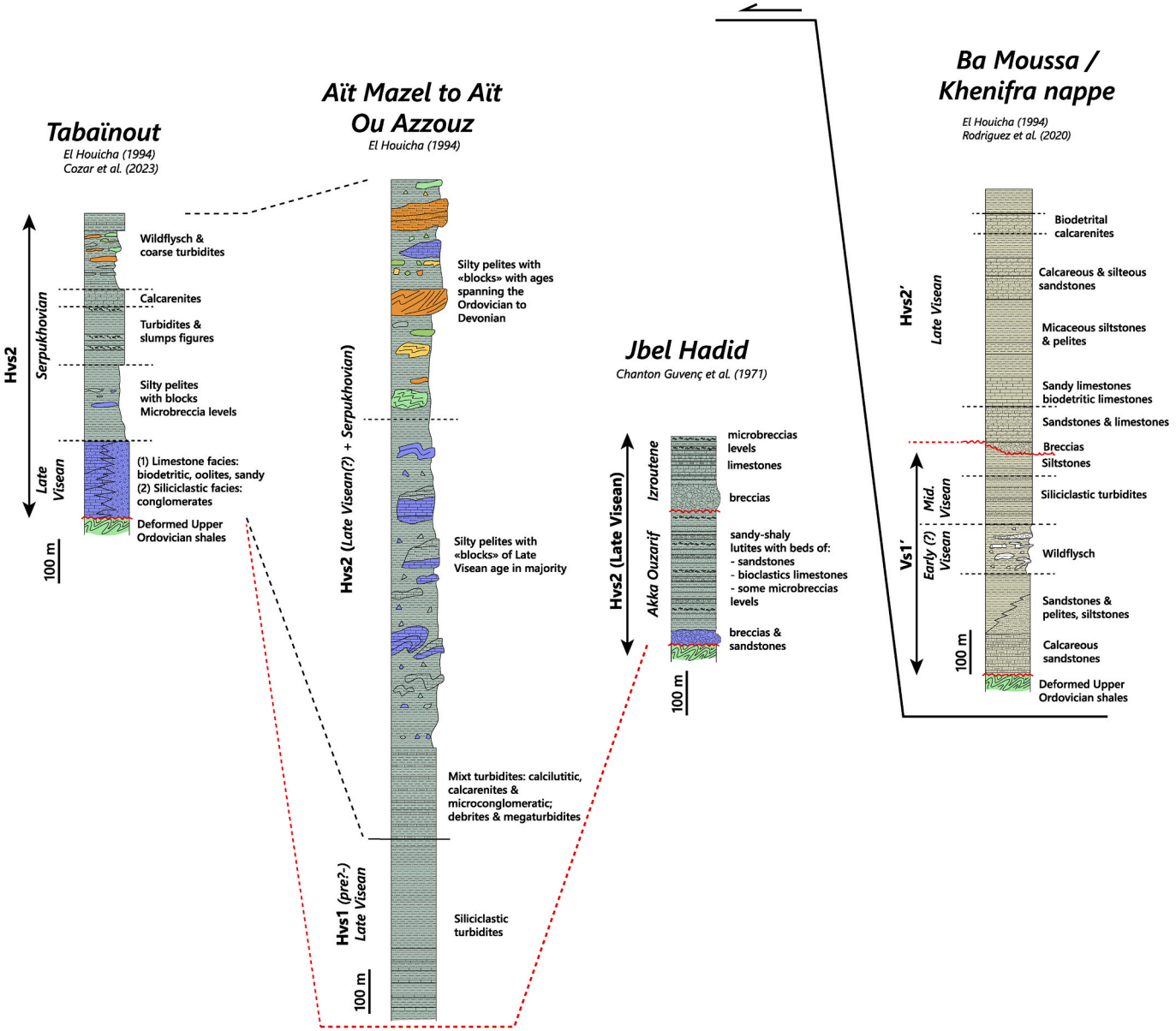

Fig. 5. Synthetic stratigraphic log of the area (after Chanton Guvenç et al., 1971; El Houicha, 1994; Rodríguez et al., 2020; Cózar et al., 2023a).

mainly reefal and bioclastic limestones; Cózar et al., 2023b) changing laterally with coarse conglomerates (blue color on Figs. 3 and 5; outcrops on Fig. 6A–B). They are followed up section by mainly siliciclastic, turbiditic deposits (Fig. 6C–D). Along the section, rare levels of mixed turbidites (siliciclastic and carbonated) can be found (Fig. 5) and within the turbiditic thick succession, reworking processes are well-evidenced (Figs. 5 and 7A-D,F). From Aït Mazel to Aït Ou Azzouz (Figs. 3 and 5) one can cross through a large part of the distal basin. Here, the serie consists in a thick succession of turbidites. Upward, these turbidites show more and more reworking processes with slumping, debrites and the occurrence of many olistholitic bodies of meter to hectometer-sizes (El Houicha, 1994, Fig. 7D). On top of a lower part mainly reworking upper Visean material, the upper part of Hvs2 reworks bigger debris of Ordovician to Devonian and Late Visean age, from pebble size to olistolith size (Figs. 5 and 7), sometimes reaching few kilometers of extension (see outcropping olistolitic masses between Tabaïnout massif and Jbel Hadid within the basin on Fig. 3, detailed in El Houicha, 1994).

Southward within the Qasbat-Tadla basin, Verset et al. (1988) also described limestones and turbiditic series, which would mainly represent the Late Visean-Serpukhovian interval. In northern continuity, one can see an important portion of reworked pebbles to olistolitic masses within a thick turbiditic succession west of Bou Acila (Fig. 2).

2.2.2. *Deformational stages*

The different stages of deformation have been summarized by Bouabdelli (1994), El Houicha (1994) and recently critically discussed in Leprêtre et al. (2024). In the Khenifra basin (autochthonous and allochthonous), lower-to upper Visean rocks are systematically

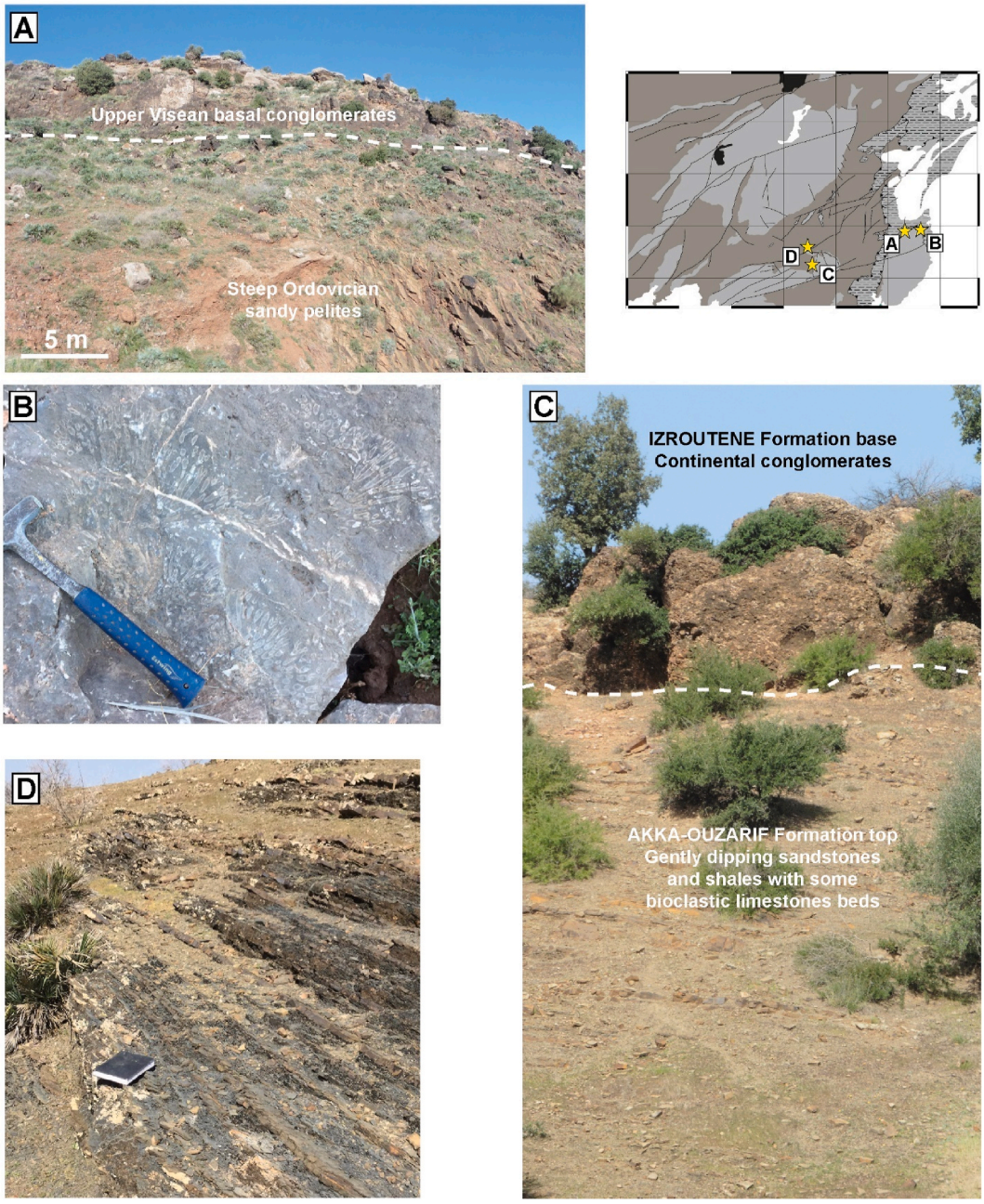

Fig. 6. Photographic plate showing the basal Visean formations. Locations on small grey-shaded map. (A) Conglomerates on top of Ordovician metapelites of Bou Guergour. (B) reefs carbonates in lateral equivalent of (A). (C) Late Visean-Serpukhovian formations on top of Jbel Hadid basement. (D) Pelitic series of Late Visean (?)-Serpukhovian in the basin.

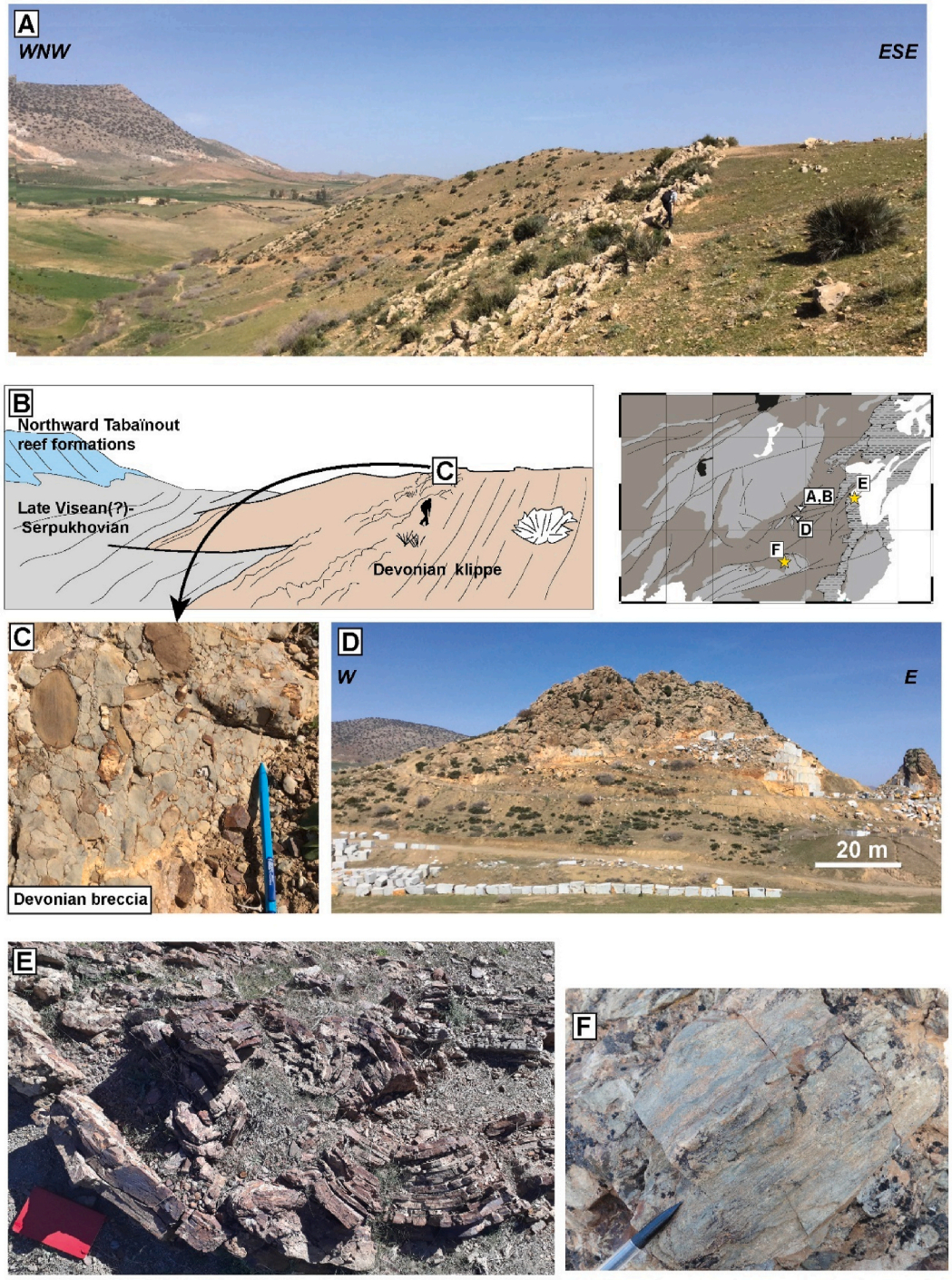

Fig. 7. Photographic plate showing the extent of reworking within the Khenifra basin, from multi-kilometric olistolith to decimetric conglomeratic pebbles. Locations on small grey-shaded map. (A) View of the eastern flank of Tabaïnout, with an upper Devonian klippe within the Khenifra sub-basin. (B) Interpreted view of (A) with a focus on a typical upper Devonian breccia facies (C). (D) View of an upper Visean carbonate olistolithic mass within the upper Visean (?)-Serpukhovian pelitic series. (E) Soft deformations within the pelitic series of the basin. (F) Reworked pebble of schistose basement rock within the conglomerates on top of the basement in Jbel Hadid.

unconformable on top of Ordovician deformed metamorphosed layers (Cózar et al., 2020, 2023a; *e.g.* Figs. 5 and 6A) and remained untouched by the Eovariscan event, be it in the autochthonous or in the allochthonous units (Bouabdelli, 1989; El Houicha, 1994).In the northern part of AKB, in Bou Khadra, Tournaisian deposits are found unconformable on Devonian rocks (Bouabdelli, 1989). Neither the Tournaisian nor the Devonian rocks show evidence of metamorphic Eovariscan deformation and the unconformity is attributed to extensional events (Bouabdelli, 1989). In the classical views (Piqué and Michard, 1989; Lahfid et al., 2019; Michard et al., 2010, 2022, 2023; Accotto et al., 2020), the Eovariscan contractional event would have taken place between Late Devonian and Early Visean, after an extensional period. Yet, alternative hypotheses have also been proposed suggesting either a fully extensional model from the end of Devonian up to Late Visean-Serpukhovian (Diot and Bouchez, 1989; Houari, 2003; Leprêtre et al., 2024) or a fully contractional model from Tournaisian onwards (Ben Abbou, 2001;

Ntarmouchant, 2003).

The Eovariscan structures generally show poorly tilted and deformed Ordovician layers (Fig. 4A; sometimes at higher angle, see Lahfid et al., 2019) showing the development of pervasive cleavage (Fig. 4B–D) at the scale of the different basement massifs. Afterwards, an extensional or transtensional event is generally recognized from Late Visean to Serpukhovian times (Huvelin, 1973; Allary et al., 1976; Beauchamp and Izart, 1987; Berkhli and Vachard, 2002; Vachard et al., 2006; *see contrasted views* in Michard et al., 2010, 2023; Bouabdelli and Piqué, 1996). At last, the first main stage of the Variscan contractional deformations occurred after the youngest deposits below the unconformable upper Pennsylvanian-Cisuralian deposits around Khenifra city (Broutin et al., 1998; Hmich et al., 2006; Domeier et al., 2021, Fig. 3). This must have occurred after Late Serpukhovian (given the stratigraphical revisions of Cózar et al., 2023a in Khenifra basin). It sets folds with vertical axial planes or slightly asymmetrical, with a general NE-SW axis direction (Fig. 8). Another hypothesis put forward by Ben Abbou et al. (2001) suggests that the Variscan compression started as soon as the Late Tournaisian, but not structural arguments can be used in favor of this model which is mainly based on sedimentological evidence.

The precise timing of the eastern nappes emplacement on top of the present day upper Visean to upper Serpukhovian formations (Fig. 4E–F, 5) is not clear but should have happened between the Late Serpukhovian/Bashkirian (El Houicha, 1994; Huvelin and Mamet, 1997) and before the main Variscan episodes that are sealed by the upper Pennsylvanian-Cisuralian deposits of the Khenifra area (Fig. 3).

3. Sampling and methods

3.1. Sampling

Sampling in the different sub-basins was done along two transects from the western to the eastern boundaries across the basin (Table 1; Fig. SD1). We collected 77 samples and maximum temperatures were determined by means of RSCM. The basinal samples are mainly Serpukhovian in age, given the recent stratigraphical revision of Cózar et al. (2023a), with the exception of Ba Moussa lower to upper Visean rocks (Cózar et al., 2020). A southern cross-section goes from Jbel Hadid to the western Ordovician basement of the Sidi Lamine Serpukhovian sub-basin (Fig. 3; A-A′). A northern cross-section starts from Bou Guergour massif and completely crosses the Khenifra upper Visean-Serpukhovian sub-basin up to the Ordovician below the Tabaïnout ridge (Fig. 3B–B'). Along these two transects, we got mainly Serpukhovian samples (but in many places the stratigraphical age is difficult to discriminate between Serpoukhovian and Late Visean; see Table 1), but also Ordovician "basement" samples, in addition to two Devonian, one Silurian and one upper Ordovician sample coming from wide klippe-olistoliths fallen into the Late Visean-Serpukhovian Khenifra sub-basin.

Targeted samples are mainly black shales (of Late Visean-Serpukhovian and Ordovician ages, but also one of Silurian age), for their higher content in organic carbon. We took care of sampling rocks that were far from highly deformed zones, where the heat and stress induced by deformation can alter the chemical nature of the organic matter (Lünsdorf et al., 2017) within the deformation structures. In line with this precaution, we also paid attention to thepotential proximity of magmatic products since volcanism has been described elsewhere, either precocious or Variscan-related (Allary et al., 1976; Birlea and Birlea, 1992; Ntarmouchant et al., 2002) and this would distort the Raman signal.

3.2. Raman spectrometry and temperature determination

3.2.1. Raman spectroscopy with organic matter

The use of Raman spectroscopy for the study of the organic matter has been carried on since the 1970s. First works aimed at studying metamorphic samples bearing graphite and its crystallinity (Tuinstra and Koenig, 1970; Wopenka and Pasteris, 1993) demonstrated the potentiality of Raman use for characterization of organic matter at high grade metamorphic conditions. As a matter of fact, Beyssac et al. (2002) demonstrated that refined examinations of the spectra allowed the calibration of a geothermometer for high-grade conditions of 330–650 °C, and that prograde crystalline re-organization of organic matter is not lost during the retrograde path. This geothermometer was later extended down by Lahfid et al. (2010) to the 200–320 °C temperature range, calibrated against well-known metamorphic series of the Glarus Alps (Switzerland), from which temperatures are known from independent methods.In these two cases, the temperature was successfully related to the relative amplitudes and positions of the main two bands of the organic matter spectra, *i.e.* the G (for "Graphite") and D (for "Disorganized") bands. The amplitudes and positions of these two bands are indeed progressively shifted as the temperature recorded increases, like the G band, shifted toward its graphitic position (Beyssac et al., 2002). Since the 2010s, the challenge has been to extend the Raman thermometer down to the diagenetic realms and in different heating rates conditions (*e.g.* near volcanic bodies or fault zones) (Wilkins et al., 2014; Schmidt et al., 2017; Schito et al., 2017, 2019, 2023; Henry et al., 2019; Muirhead et al., 2020).

Fig. 8. Variscan folds affecting the upper Visean (?)-Serpukhovian pelitic series of the Khenifra sub-basin.

Table 1
RSCM results. Long: longitude; lat: latitude.

Sample name	Stratigraphic age	Rock type	Long	lat	Mean Temp (°C)	Standard deviation (°C)	Nb of spectra
J3-1ord	Early-mid. Ordov.	sandy shales	−5.857699	32.81238	272	9	30
J3-2ord	Early-mid. Ordov.	sandy shales	−5.857685	32.812427	268	10	43
J3-3Vis	Upp. Vis-Serpukh.	conglo-sandstones	−5.855682	32.812961	343	52	42
J3-4Vis	Upp. Vis-Serpukh.	conglo-sandstones	−5.857148	32.815048	253	46	39
J3-6Vis	Upp. Vis-Serpukh.	sandstones	−5.846208	32.819225	267	27	46
J3-9ord	Early-mid. Ordov.	sandy shales	−5.843854	32.841979	282	9	22
J3-10Vis	Upp. Vis-Serpukh.	grey-black shale	−5.843359	32.849829	259	10	22
J3-11Vis	Upp. Vis-Serpukh.	grey-black shale	−5.843137	32.851538	232	11	20
J3-12Vis	Upp. Vis-Serpukh.	grey-black shale	−5.844757	32.857636	233	8	28
J3-13Vis	Upp. Vis-Serpukh.	grey-black shale	−5.860712	32.860417	184	55	47
J3-14Vis	Upp. Vis-Serpukh.	grey-black shale	−5.867652	32.8636	178	46	40
J3-16Vis	Upp. Vis-Serpukh.	grey-black shale	−5.889403	32.882003	172	26	21
J3-17Vis	Upp. Vis-Serpukh.	grey-black shale	−5.890148	32.896515	222	8	14
J3-18Vis	Upp. Vis-Serpukh.	grey-black shale	−5.906088	32.901333	213	23	19
J3-19ord	Upp. Ordov.	shale	−5.912893	32.904089	246	16	25
J3-21Vis	Upp. Vis-Serpukh.	grey-black shale	−5.91282778	32.904	224	30	17
J4-1ord	Upp. Ordov.	shale	−5.843128	32.949067	265	14	27
J4-2Vis	Upp. Vis-Serpukh.	grey-black shale	−5.841925	32.948476	132	18	22
J4-3Vis	Upp. Vis-Serpukh.	grey-black shale	−5.818061	32.958025	149	9	16
J4-4Vis	Upp. Vis-Serpukh.	grey-black shale	−5.82107	32.9505	141	12	16
J4-5Vis	Upp. Vis-Serpukh.	grey-black shale	−5.816026	32.949417	160	15	20
J4-6Vis	Upp. Vis-Serpukh.	grey-black shale	−5.815496	32.94992	149	19	20
J4-7Dev	Upp. Devonian	shale	−5.81316	32.949326	209	9	26
J4-8Dev	Upp. Devonian	shale	−5.806741	32.953757	183	10	24
J4-9Vis	Upp. Vis-Serpukh.	grey-black shale	−5.81725	32.938934	153	20	11
J4-10sil	Silurian	black shale	−5.827337	32.923571	141	20	30
J4-11ord	Upper Ordovician	shale	−5.828511	32.926507	148	18	24
J4-12Vis	Upp. Vis-Serpukh.	grey-black shale	−5.832333	32.925018	172	18	24
J4-15Vis	(pre?)-upp. Visean	sandy shale	−5.784613	32.947097	207	15	19
J4-16Vis	(pre?)-upp. Visean	sandy shale	−5.780348	32.942751	215	12	17
J4-17Vis	(pre?)-upp. Visean	sandy shale	−5.776689	32.942734	241	12	23
J4-18Vis	(pre?)-upp. Visean	sandy shale	−5.773888	32.942601	222	10	20
J4-21Vis	Upp. Vis-Serpukh.	grey-black shale	−5.759602	32.943202	218	7	21
J4-22Vis	Upp. Vis-Serpukh.	grey-black shale	−5.752927	32.944879	204	11	23
J4-23Vis	Upp. Vis-Serpukh.	grey-black shale	−5.752927	32.944879	206	8	17
J4-24Vis	Upp. Vis-Serpukh.	grey-black shale	−5.75016	32.945863	200	11	21
J5-1ord	Upper Ordovician	shale	−5.972331	32.915202	247	4	30
J5-2Vis	Upp. Vis-Serpukh.	conglo-sandstones	−5.988666	32.912956	241	14	20
J5-3ord	Upper Ordovician	shale	−6.013087	32.904597	229	16	22
J5-4Vis	Upp. Vis-Serpukh.	grey-black shale	−6.01309	32.904572	257	14	20
J5-5Vis	Upp. Vis-Serpukh.	grey-black shale	−6.031629	32.905911	213	16	20
J5-6ord	Upper Ordovician	shale	−6.098944	32.919569	290	14	23
J5-7ord	Upper Ordovician	shale	−6.097151	32.920437	288	14	20
J5-8Vis	Upp. Vis-Serpukh.	grey-black shale	−6.073828	32.919233	143	16	18
J5-9Vis	Upp. Vis(?)-Bashkir.	shale	−6.053502	32.917297	142	15	18
J5-10Vis	Upp. Vis-Serpukh.	grey-black shale	−6.047117	32.911349	182	9	20
J6-1Vis	Lower-Mid. Visean	shales, silts, sdst.	−5.685702	32.953165	234	15	22
J6-2Vis	Lower-Mid. Visean	shales, silts, sdst.	−5.691763	32.964121	237	12	20
J6-3Vis	Lower-Mid. Visean	shales, silts, sdst.	−5.696756	32.968547	234	15	21
J6-4Vis	Lower-Mid. Visean	shales, silts, sdst.	−5.703093	32.971263	205	19	21
J6-5vis	Lower-Mid. Visean	shales, silts, sdst.	−5.704465	32.970937	209	18	20
J6-6Vis	Lower-Mid. Visean	shales, silts, sdst.	−5.703163	32.972307	230	16	21
J6-7Vis	Lower-Mid. Visean	shales, silts, sdst.	−5.70307	32.972364	230	9	24
J6-8Vis	Lower-Mid. Visean	shales, silts, sdst.	−5.706628	32.971687	216	11	21
J6-9Vis	Lower-Mid. Visean	shales, silts, sdst.	−5.711571	32.969032	212	8	26
J6-10Vis	Lower-Mid. Visean	shales, silts, sdst.	−5.710528	32.970363	213	11	21
J6-11Vis	Upper Visean	siltstone	−5.698842	32.966564	231	14	25
J6-13Vis	Lower-Mid. Visean	shales, silts, sdst.	−5.684018	32.938186	242	10	22
J6-16Vis	Upper Visean	siltstone	−5.68666	32.935025	249	10	24
J6-17Vis	Upper Visean	siltstone	−5.692487	32.930803	253	18	22
J6-18Vis	Upper Visean	siltstone	−5.693326	32.929981	232	12	16
J6-20Vis	Upper Visean	siltstone	−5.696181	32.928829	241	10	19
J7-1ord	Early-mid. Ordov.	sandy shale	−5.670242	32.891522	301	19	26
J7-3ord	Upper Ordovician	shale	−5.671877	32.899503	250	5	26
J7-4ord	Upper Ordovician	shale	−5.6817	32.926006	247	8	34
J7-5ord	Upper Ordovician	shale	−5.690955	32.902196	275	6	33
J7-6Vis	(pre?)-upp. Visean	sandy shale	−5.699099	32.904059	246	10	22
J7-7Vis	Upp. Vis-Serpukh.	grey-black shale	−5.716839	32.909741	229	10	20
J7-8ord	Upper Ordovician	shale	−5.709437	32.945613	221	8	20
J7-9Vis	Upp. Vis-Serpukh.	grey-black shale	−5.712113	32.952738	216	10	25
J7-10Vis	Upp. Vis-Serpukh.	grey-black shale	−5.745732	32.938083	202	12	20
J7-12Vis	Upp. Vis-Serpukh.	grey-black shale	−5.735319	32.940605	203	9	22
J7-13Vis	Upp. Vis-Serpukh.	grey-black shale	−5.73322222	32.93933889	208	18	28
J7-15Vis	Upp. Vis-Serpukh.	grey-black shale	−5.732075	32.938393	219	10	20

(*continued on next page*)

Table 1 (*continued*)

Sample name	Stratigraphic age	Rock type	Long	lat	Mean Temp (°C)	Standard deviation (°C)	Nb of spectra
J7-16Vis	Upp. Vis-Serpukh.	grey-black shale	−5.722351	32.929923	227	10	20
J7-17Vis	Upp. Vis-Serpukh.	grey-black shale	−5.726354	32.932383	225	10	19
J7-18Vis	Upp. Vis-Serpukh.	grey-black shale	−5.728687	32.935297	226	8	25

3.2.2. *Treatment and temperature determination*

Raw samples were crushed and surficially altered parts were removed. Raman measurements were realized in the I-Mat experimental platform (CY Cergy Paris Université, MIR) with a Witec Raman equipped with Nd-YAG 532 nm laser and x50 objective on optical microscope. Power was set between 1 and 5 mW. We used gratings of 1200 lines/mm.

For temperature determination, we use the procedure detailed by Lünsdorf et al. (2017; 2016). It consists in a peak-fitting procedure using pseudo-Voigt functions. In details, we used at least 25–30 spots for Raman spectroscopy on each sample, then applied the Lünsdorf et al. (2017) method. We thus obtained 25–30 values of individual temperatures for each spot. A distribution histogram was realized for each sample, in order to check for consistency among all analyzed spots. In some siliciclastic samples, extreme out-of-trend high temperatures values were found due to the presence of reworked carbonaceous material that was definitely excluded from mean temperature calculation. For other samples, the temperature distribution was relatively spread. In these cases, we first carefully checked the consistency among the spectra

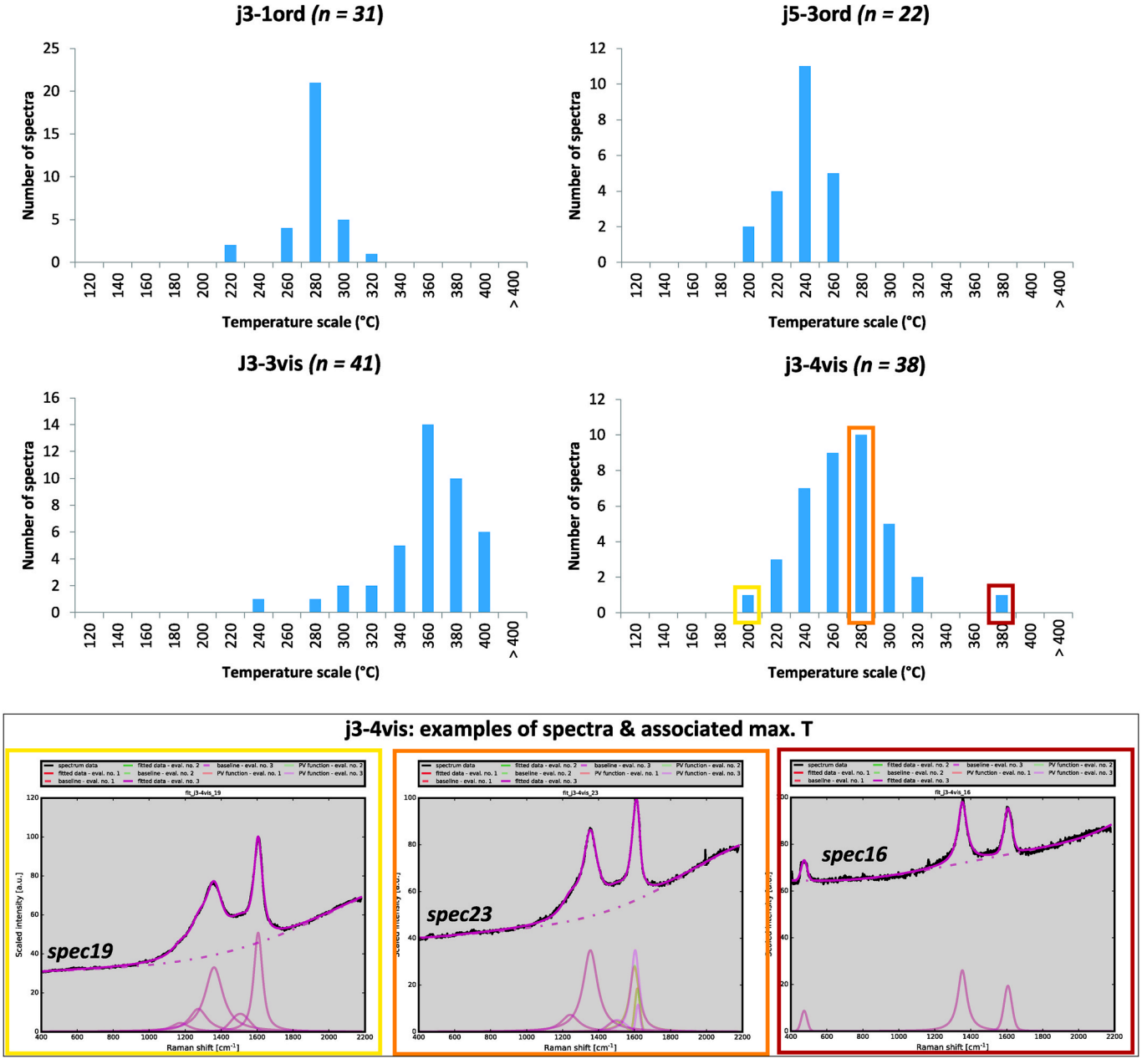

Fig. 9. *On top:* example of temperature distribution histograms for, on one hand the case of a single well-defined population and, on the other hand, for a very detrital sample, showing a lot of reworking. *On the bottom:* examples of characteristic spectra for each temperature range. Black noisy line: real spectra; light purple line: de-noised spectra; pink multiple bands: band decomposition of the light purple de-noised spectra.

shapes to ascertain similarities and the presence of one population of spectra shapes. Then, we used a cut-off value excluding 5–10% of the extreme temperature values within the distribution. Ultimately, we used a minimum of 15 spectra for each sample to obtain a good reproducibility of the temperature determination. In Table 1, we present the results with the mean temperature, associated with the standard deviation calculation. Raw data can be found within the Supplementary Data files.

3.3. Geochemical data from the Qasbat-Tadla basin

Geochemical data on organic matter from the Qasbat-Tadla has been published into few studies (Jabour and Nakayama, 1988; Er-Raïoui et al., 2001). We will use mainly the data from Rock-Eval Pyrolysis analyses. We discard the vitrinite reflectance (Ro) dataset from Jabour and Nakayama (1988) since they did not provide the raw Ro measurements files and thus we do not know if they carefully differentiated autochthonous and allochthonous organic matter particles, which is a well-known bias that can artificially increase the Ro value (Senftle and Landis, 1991). We also did not use the Hydrogen Index (HI)/T_{max} values of Er-Raïoui et al. (2001) for Boujad-101 and Boujad-104 well since we could not properly access the raw data to separate them in terms of stratigraphy and burial depth.

Regarding data interpretation, we excluded many data points for the following reasons. First, the low TOC content (<1%) is problematic when it comes to Rock-Eval analyses because it will give too low signal for precise measurements of the S2 peak, inducing error in the appreciation of T_{max} and HI. Second, the Mineral Matrix Effect (MME), responsible at low TOC (<3%) for an artificial decrease of HI (Espitalié et al., 1980; Katz, 1983) makes some datapoints not suitable for interpretation before a correction. This correction has been taken into account to adjust the measured HI and T_{max} values.

4. Results

4.1. Temperatures from RSCM geothermometer

Raman spectra in this work are heterogeneous showing different shapes as drawn in Fig. 9. In low maturity spectra (Fig. 9, bottom left) the D band shows lower intensities with respect to the G band and a shoulder at about 1250 cm^{-1}. The almost symmetric peak at 1600 cm^{-1} can be treated as a broad composite G band, as it is not possible to separate the G and D2 bands in poorly organized carbon in low-grade metamorphic rocks (Beyssac et al., 2002). At higher maturity ranks spectra show a broader D band with high intensities and a slightly asymmetrical G band (Fig. 9, bottom center). Finally, the highest temperature spectra in the area are characterized by a D and G bands showing progressively similar intensities (Fig. 9, bottom right) and for T > 350 °C it will also show strongly asymmetrical G bands with a clear shoulder at 1620 cm^{-1} (D2 band; see Supplementary Data files).

It is worth noting that for some Late Visean-Serpukhovian samples (j3-3vis, j3-4vis & j3-6vis), it was difficult or impossible to find a single homogeneous population allowing the calculation of a “real” mean temperature. In these cases, spectra are heterogeneous because of the multiple origins of the organic matter particles that were analyzed (Fig. 9; j3-4vis as an example). Indeed, these samples were mostly collected within siliciclastic rocks with significant reworking as for instance in the basal upper Visean conglomerates where a lot of deformed Ordovician pebbles have been observed (like on Fig. 6A and C). For these samples, the mean temperature is given in Table 1 but does not have a direct meaning for geological interpretation. Given the reworking comes from the erosion of older rocks, it tends to provide organic matter particles that experienced higher temperatures than the “real” temperature experienced by the considered sample. Hence, the mean temperature for these detrital samples most often represents an over-estimate of the “real” temperature reached by the sample in the course of its history (if it had never been thermally overprinted later).

RSCM temperatures for each sample are presented in detail in Table 1 and plotted on map and cross-section views (Figs. 3 and 10, respectively). They are also represented as histogram distributions for the Ordovician samples on one hand and for the Upper Visean-Serpukhovian samples, on the other hand (Fig. 11A).

Table 1 and Fig. 3 show quite well that temperatures range from low values of 132 ± 18 °C or 143 ± 16 °C (samples j4-2vis and j5-8vis, respectively) to higher values of 301 ± 19 °C or 290 ± 14 °C (samples j7-1ord and j5-6ord, respectively). Comparing upper Ordovician with Carboniferous samples (Fig. 11A), it can be observed that upper Ordovician samples show a 229 ± 16 °C (j5-3ord) to 301 ± 19 °C (j7-1ord) temperature range, whereas the temperature range for Carboniferous samples (samples with homogeneous spectra population)is larger, going from 132 ± 18 °C (j4-2vis) up to 259 ± 10 °C (j3-10vis). In details, Upper Ordovician samples from the western basin boundary (Zaian massif) and from the eastern basin boundary (from the allochthonous Khenifra nappe & Bou Guergour massif) show barely the same temperatures (Fig. 11B). At last, four temperatures were determined from Devonian and Silurian-Late Ordovician olistolites-klippe samples with average RSCM temperatures of 148 ± 18 °C (j4-11ord), 141 ± 20 °C (j4-10sil), 183 ± 10 °C and 209 ± 9 °C (j4-8dev and j4-7dev, respectively).

With respect to the spatial distribution of the RSCM temperatures, we will describe them following our two representative cross-sections (Fig. 10).

The southern A-A′ cross-section cuts across the northern Sidi Lamine sub-basin, the Oulad Bacha Fault, the SE Zaian massif, the southern Khenifra sub-basin up to the Jbel Hadid after crossing the Targa n'Ali Fault (Fig. 3). Across the north of the Sidi Lamine sub-basin, from west to east, we first have a western sharp contact between Ordovician samples j5-6ord and j5-7ord, with 290 ± 14 °C and 288 ± 14 °C, respectively and Serpukhovian samples j5-8vis, with 143 ± 16 °C, in line with the Takkat S. and Takkat N. samples of Lahfid et al. (2019) displaying temperatures of ~160 °C. Temperatures from Carboniferous samples increase by *ca.* 100 °C toward the east, reaching 257 ± 14 °C (j5-4vis)/264 ± 9 °C (S. Lamine [Lahfid et al., 2019]). The Ordovician eastern boundary of Sidi Lamine sub-basin (Oulad Bacha Fault) shows temperatures spreading from 229 ± 16 °C (j5-3ord) to 295 ± 8 °C (S. Ifouloussene [Lahfid et al., 2019]). From Kef N'Sour toward the east, Ordovician samples show temperatures of 247 ± 4 °C (j5-1ord), 246 ± 16 °C (j3-19ord), or 290 ± 9 °C (Kef N'Sour in Lahfid et al. [2019]). Upper Visean-Serpukhovian samples close to the Ordovician basement have comparable but slightly lower temperatures: from 213 ± 23 °C to 241 ± 14 °C (j5-2vis, Oulad Bacha [Lahfid et al., 2019], j3-18vis). Then across the southern Khenifra sub-basin (Aït Ou Azzouz; Fig. 10), the youngest samples from Hvs2 formation have the coldest temperatures (172 ± 26 °C to 184 ± 55 °C; see map Fig. 3). Toward the eastern end of this cross-section, approaching the Jbel Hadid (Izroutene Fm.), Carboniferous samples (j3-10/11/12vis) show temperatures from 232 ± 11 °C to 259 ± 10 °C, unconformable on Ordovician samples that show higher temperatures from 268 ± 10 °C to 282 ± 9 °C (j3-1/2/9ord). Belonging to the upper Visean detrital formations resting unconformable on the Ordovician ones, samples j3-3/4/6vis show very widespread temperature values (due to their highly detrital content) which cannot be considered for geological interpretation.

The northern B-B′ cross-section goes from the Tabaïnout area to Khenifra, across the center of Khenifra sub-basin (Fig. 3). The Ordovician sample directly below the Tabaïnout reef shows a 265 ± 14 °C temperature (j4-1ord) which is significantly hotter than the closest Carboniferous sample, showing 132 ± 18 °C (j4-2vis). Between the Tabaïnout and the Aït Mazel anticline dome, sampled Hvs1 and Hvs2 formations show temperatures from 141 ± 12 °C to 160 ± 15 °C (j4-3/4/5/9vis). Ordovician, Silurian samples from olistolites-klippen embedded within the Hvs2 formation show 141 ± 20 °C (j4-10sil) to 148 ± 18 °C (j4-11ord) temperatures, within the temperature range of the Hvs2 samples. On the opposite, Devonian samples from the northern olistolitic bodies have 183 ± 10 °C and 209 ± 9 °C (j4-8dev and j4-7dev,

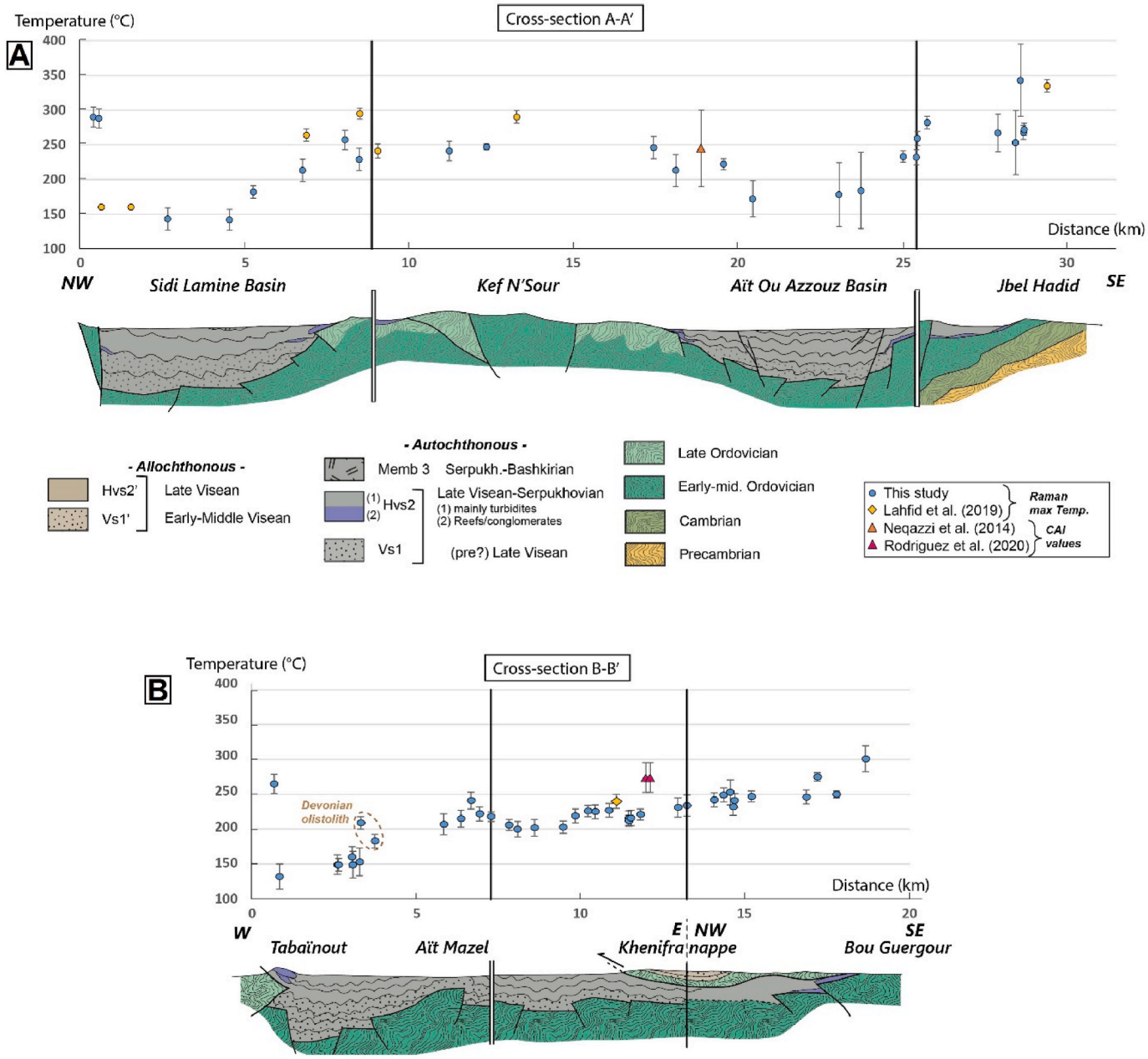

Fig. 10. cross-sections along the two sampled transects with thermal results. (A) on the top: southern transect A-A': from Jbel Hadid to Sidi Lamine sub-basin. (B) on the bottom: northern transect B-B': from Khenifra to Jbel Tabaïnout. Plotted on top of each cross-section are the temperatures obtained through Raman spectra analysis. Precise names and locations for these specific samples are given in Fig. SD1.

respectively), significantly higher than the surrounding Hvs2 samples. Eastward, the temperature evolution mimics the alternation between the Aït Mazel anticline Hvs1 and younger Hvs2 formations to the east. Maximum temperatures are reached within the anticline core from 218 ± 7 °C to 241 ± 12 °C (j4-17/18/21vis) compared to colder ones outside of it from 200 ± 11 °C to 206 ± 8 °C (j4-23/24vis, j7-10/12vis). At last, the easternmost part of the cross-section belongs to the Khenifra nappe, bearing the Jbel Ba Moussa syncline. There, the allochthonous Ordovician and lower to upper Visean samples (j7-4/8ord, j6-1vis and j7-9vis) show 216 ± 10 °C and 247 ± 8 °C temperatures that are very similar to the temperature range of the Jbel Ba Moussa Hvs2' samples (j6-16/17/18/20vis and j6-13vis), with temperature range of 232 ± 12 °C to 253 ± 18 °C. Thus, allochthonous Visean and upper Ordovician samples show similar temperatures.

Out of the cross-section trace, the RSCM temperatures are largely overlapping and consistent within the northern allochthonous Vs1′Carboniferous samples (j6-2/3/5/7/8/9/11vis) showing a 209 ± 18 °C to 237 ± 12 °C temperature range (not projected on cross-section). Moreover, along the nappe contact, autochthonous Carboniferous samples (j7-6/7/16/17vis) show a 225 ± 10 °C to 246 ± 10 °C range, to be compared to the overlapping 221 ± 8 °C to 275 ± 6 °C range of allochthonous Ordovician samples (j7-3/5/8ord). Finally, the autochthonous Bou Guergour Ordovician massif gave one sample (j7-1ord) with a significantly higher temperature of 301 ± 19 °C.

4.1.1. Geochemical data

The geochemical data are presented on Fig. 12. They are differentiated according to their stratigraphy. They show two good records of Paleozoic rocks from the Kasbat-Tadla-1 (KAT-1) and Boujad-105 wells. In the KAT-1 well, from 300 to 1350 m of depth, the TOC range from

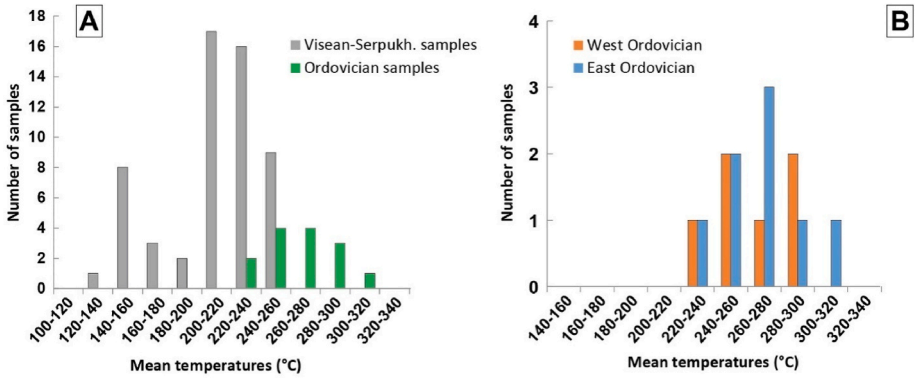

Fig. 11. Temperatures distribution histograms. (A) Temperatures distribution for the Visean-Serpukhovian and Ordovician samples; (B) Temperatures distribution for the western and eastern Ordovician samples.

almost none to 9 % for the Devonian levels (300–700 m of present-day burial), from 3 to 13% for the Silurian ones (720–800 m of burial) and from 0.5 to 6 % for the Ordovician ones (800–1350 m of burial). In the Boujad-105 well, from 600 to 1000 m of depth, Devonian and Ordovician levels show TOC <1 % and are thus not suitable for interpretation. In between (800–960 m of present-day burial), Silurian levels span a 0.5–8.5 %. A third well, KAT-2, is also available, but no T_{max} data are associated to the samples so that the maturity remains out of reach. Contrastingly, this well shows much less important TOC, but it sampled less of the Devonian to Ordovician levels. They are in the range of 0.5–2 % of TOC for Devonian and Silurian levels. Carboniferous levels show very low TOC from 0 to 1 %.

The KAT-1 and Boujad-105 geochemical data can be used with good confidence for having many samples showing TOC >2–3% (MME effect). ***For the Boujad-105 well***, T_{max} can be considered with confidence only for the Silurian levels, between 900 and 1000 m, where they range from 449 to 455 °C, with one single anomalous value with low Hydrogen Index value, showing a significantly lower T_{max} value. ***For the KAT-1 well***, T_{max} are grouped between *ca.* 439 and 446 °C with low-TOC or low-Hydrogen index samples having scattered values around. In this area, Ordovician to Devonian rocks are representative of type-II/type-III source rocks. Silurian source-rock can be considered as a type II, as it is a well-known marine-derived organic matter (Boote et al., 1998). Silurian levels show T_{max} ranging from 438 to 444 °C with associated HI values of *ca.* 200–320 mg/g C. Ordovician levels are more scattered, with a majority of samples with TOC >2 % and HI of 100–250 mg/g C having a T_{max} range of 441–447 °C. In the case of the Ordovician samples, it is interesting to note that good TOC levels are either at the base (*ca.* 1300–1350 m of burial) or the top (800–950 m) of the Ordovician sedimentary pile. In details, for these two groups of samples the T_{max} ranges are not possible to discriminate but their HI evolution is quite different, with a mean HI of 200–220 mg/g C for the top group, against a mean HI range of 110–130 mg/g C. With a depth difference of 350–450 m between the two Ordovician TOC-rich levels, it means either that the precursors were somehow different between the Ordovician source rocks, and they share similar maturities or that within this undiscernible T_{max} range, samples from the bottom were somehow slightly more mature, having lost more of their S2 peak signal. At last, Devonian levels show two trends. One trend has only three samples showing good TOC (>2%) and HI. Anyway, these samples are suspicious. Together with the MME correction, these points show a mean HI ~500 mg/g C with T_{max} between 443 and 449 °C. The problem is that such elevated values of T_{max} mean that the initial kerogens have already undergone significant transformation ratios that are not compatible with the preservation of such high HI values (expected to reach values < 200–300 mg/g C). Devonian data from this trend will thus not be used. The second trend shows HI range of 200–250 mg/g C, for samples coming from the whole Devonian section thickness. The samples belonging to this trend show T_{max} values ranging from 442 to 446 °C. We will thus mainly use the homogeneous pool of Ordovician, Silurian and Devonian (2nd trend) samples maturity data for the discussion. We will keep in mind that these overlapping T_{max} ranges are surprising for a sampled thickness of 1 km, but we can consider that it gives us a mean signal.

5. Discussion

The distribution of the RSCM temperatures and the organic matter geochemical results will now be discussed in relationship with the available geological information, in order to answer two questions related to: (1) the timing of acquisition and (2) the mechanisms/models we should use in order to explain the observed results.

5.1. General thermal constraints for interpretation

In order to discuss whether or not our results are compatible with a Late Paleozoic age for maturity acquisition, we first examine the intensity of reheating during the Mesozoic-Cenozoic burial. Second, based on our new results, bibliographical and field geology arguments, we shall discuss the timing of acquisition, be it Late Paleozoic or Mesozoic-Cenozoic. This second point will be treated in the following sections.

Regarding the first point, the Western Meseta has undergone a succession of vertical motions during the Mesozoic-Cenozoic. Different low-temperature thermochronology studies on apatite have been realized in the Rehamna, the Jebilet and the MCM (Ghorbal et al., 2008; Saddiqi et al., 2009; Barbero et al., 2011, Fig. 1). In particular, for the MCM, Barbero et al. (2011) modelled thermal paths with post-Paleozoic temperatures generally never higher than 80 °C (with the exception of one sample, RO7, showing Triassic reheating up to 130 ± 10 °C, that cannot lean on field evidence and should be taken with caution). These results are similar and consistent with what has been described by Ghorbal et al. (2008) and Saddiqi et al. (2009) on the Rehamna and Jebilet further south.

Compared to the RSCM temperatures (this study and Lahfid et al., 2019) almost exclusively higher than 140 °C for the upper Visean-Serpukhovian rocks (only one sample, j4-2vis, has a 132 ± 18 °C RSCM temperature <140 °C) and >229 °C for Ordovician rocks (j5-3ord; Fig. 11A; Table 1), it can be concluded that all rocks within the southern AKB acquired their thermal signature well before the Mesozoic.

In the case of the Qasbat-Tadla basin, our quality check on the data showed that the samples from KAT-1 and Boujad-105 wells, reached T_{max} values of 438–447 °C and 449–455 °C, respectively. It is worth noticing that these T_{max} values were reached for present-day depths varying between 900 and 1000 m for Boujad-105 well and 400–1400 m for KAT-1 well. In order to be exploitable as maximum maturity depth, the T_{max} values should be translated into equivalent temperature ranges, so that given a chosen paleo-geotherm we can derive estimates of

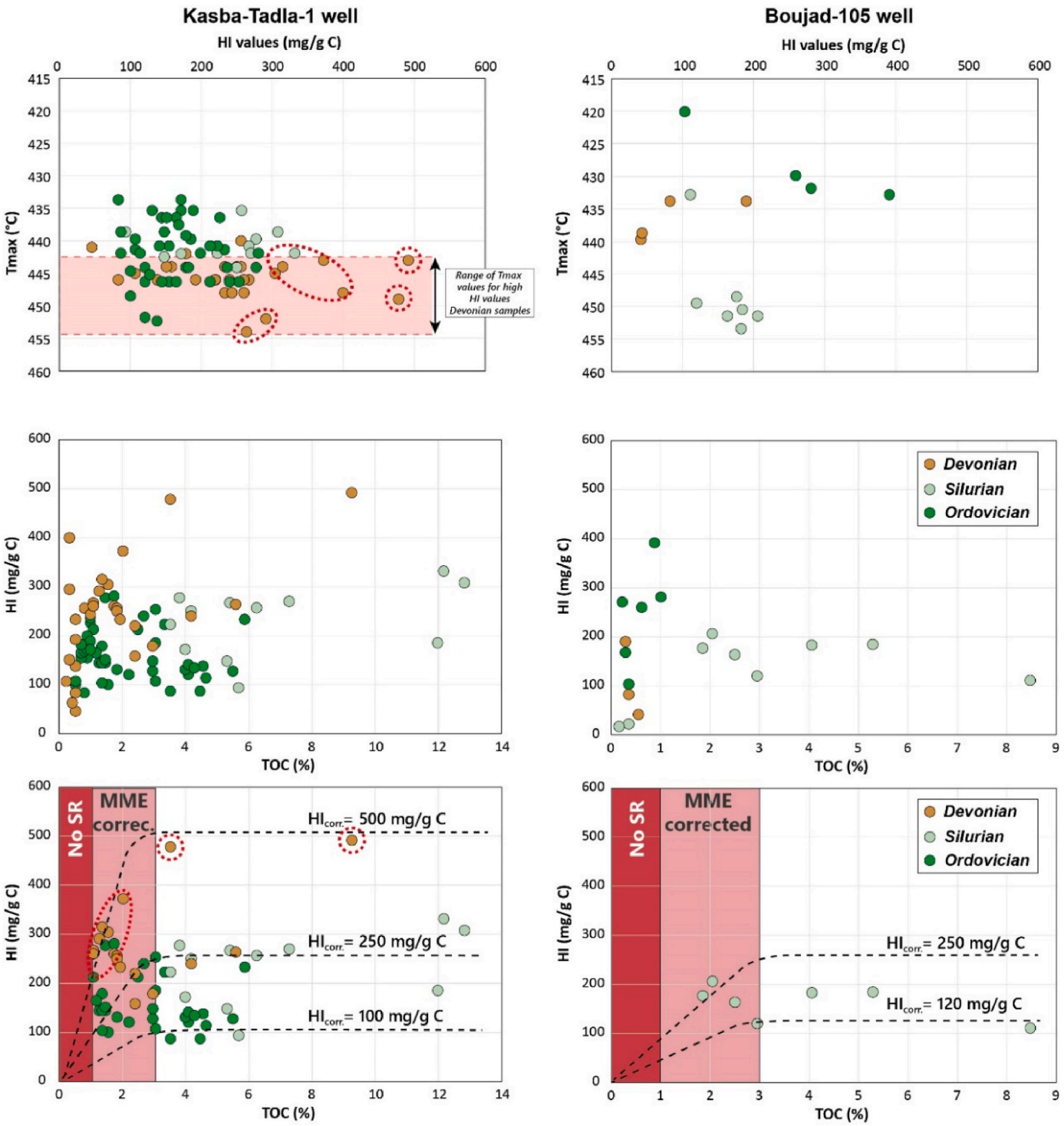

Fig. 12. Geochemical data from KAT-1 and Boujad-105 wells.

maximum burial. We can follow the conversion scale of Petersen et al. (2013) for the conversion of T_{max} into Ro equivalent for graptolite-bearing shales. For the Silurian samples of both the KAT-1and Boujad-105 wells, this gives 0.8–0.9 % Ro_{eq} and 1–1.2 % Ro_{eq}, respectively. Then, using different Ro-temperature conversion models, we can estimate temperature ranges for these two maturity ranges. By using the classical EasyRo model of Sweeney and Burnham (1990), it gives rough estimates of 110–130 °C for samples of KAT-1 well and 140–160 °C for samples of Boujad-105 well. With the more recent basin%Ro model of Nielsen et al. (2017), we got 150–160 °C for the KAT-1 samples and 170–175 °C for Boujad-105 samples. In these two wells, the Paleozoic rocks are buried below few hundred meters of Mesozoic-Cenozoic deposits (Verset et al., 1988).

Given the apatite low-temperature thermochronology constraints, the maximum Mesozoic-Cenozoic reheating up to 80–90 °C can not be responsible for the maturities recorded by the Paleozoic rocks in the Qasbat-Tadla basin. We thus consider that the recorded maturities were attained during Paleozoic. Anyway, in the case of the Qasbat-Tadla basin, the limited distribution of results and the impossibility to estimate paleo-geotherms make it a difficult case for determining the

acquisition timing of maturities. We only know that maturities were acquired during Late Paleozoic but are unable to discriminate between pre-Variscan or Variscan timing.

5.2. Thermal maturities in the Khenifra basin

5.2.1. Acquisition timing for the RSCM temperatures

5.2.1.1. A short summary of the hypotheses. The major problem of interpreting the RSCM temperatures is that we do not benefit from subsurface geometries. We only have surface samples that are thought to tell a common story for the area. As such, the western and eastern boundaries of the Khenifra basin are giving us a puzzling a priori difference (Fig. 13). On one hand (Fig. 13A), the western boundary shows us a net and significant temperature gap (ΔT~80–150 °C) between the upper Visean-Serpukhovian and Ordovician rocks that tends to suggest a two-step story: a first phase with low-grade metamorphism affecting the Ordovician rocks and a second phase with the development of the basin within a colder environment giving lower final temperatures for the upper Visean-Serpukhovian rocks. On the other hand (Fig. 13B), the eastern boundary is at odds with the former. A single-phase story is simpler here: rocks reached their thermal maximum together, either (1) during a stage when the Eovariscan deformation and basin development were more or less synchronously active (exhumation of Ordovician basement and basin infill) or (2) during the Variscan stages, between the end of Pennsylvanian and Cisuralian. Three lines of argument are presented below in order to discuss these two hypotheses.

5.2.1.2. RSCM temperatures distributions and geometrical arguments.

- **Similar temperature ranges for Ordovician basement**

For all Ordovician samples, we observe overlapping similar temperature ranges, for both sides of the basin (Fig. 11B). In addition, these thermal similarities are consistent with a previous illite crystallinity study (Bouabdelli, 1994, Fig. 14). This goes consistently with the fact that the Eovariscan deformation affected the Ordovician series within a similar low-grade metamorphic gradient, setting similar types of deformation (Allary et al., 1976; Bouabdelli, 1989; El Houicha, 1994). The thermal and structural observations are in agreement with the

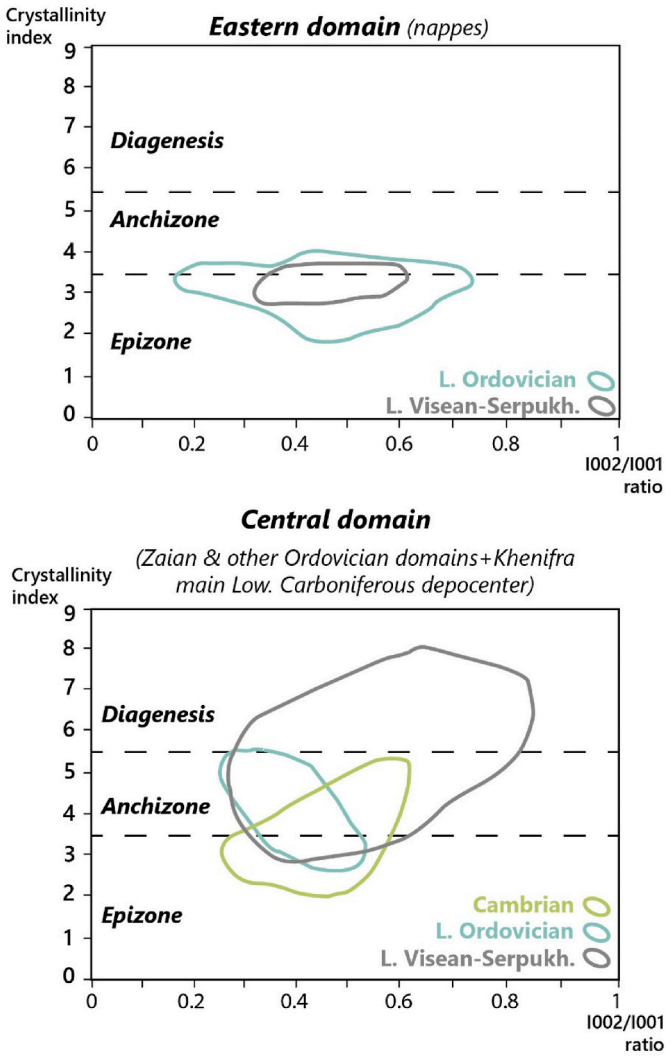

Fig. 14. Illite crystallinity data from Bouabdelli (1982).

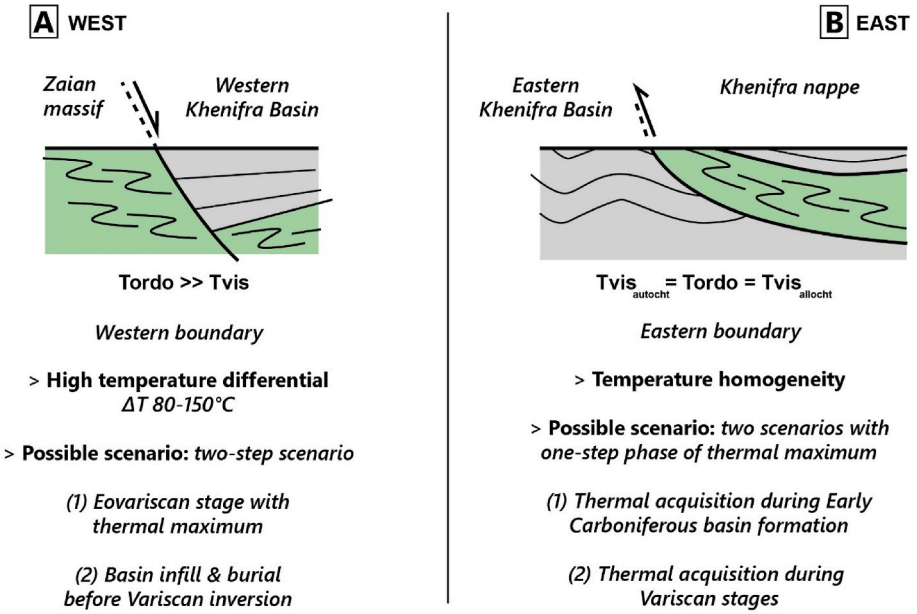

Fig. 13. Sketches summarizing the hypotheses for the thermal acquisition in the Khenifra sub-basin, given the western or eastern point of view.

acquisition of maturities during one main tectono-metamorphic event.

- **Overlapping lower Carboniferous/Ordovician RSCM temperatures in the east**

On section B-B′, to the east, RSCM temperatures of Visean and/or Serpukhovian and Ordovician rocks show undistinguishable values (Figs. 10 and 13B). To a lesser extent, close to Jbel Hadid (section A-A'), Visean and/or Serpukhovian rocks RSCM temperatures increase and almost reach the Ordovician temperatures. Two scenarios are acceptable: (1) both Ordovician and Visean and/or Serpukhovian rocks acquired a common maturity at the time of the Eovariscan deformation/basin deepening; (2) post-"Eovariscan deformation" events were hot enough for Visean and/or Serpukhovian rocks to reach the previous Eovariscan thermal maxima. This second scenario implies two additional hypotheses that are: (i) to have precisely heat the Visean and/or Serpukhovian rocks to the maturity levels of the Ordovician ones (recorded in Zaian Mountains too) and (ii) this maturation should have been localized only in the eastern part of the basin, and not everywhere. For now, we favor the scenario (1) to not overcomplicate.

- **Thermal stratification consistent with stratigraphical successions**

On both cross-sections, in the synforms of Sidi Lamine, Aït Ou Azzouz and between Tabaïnout and Aït Mazel, the RSCM temperatures are consistently lower in the stratigraphically younger core of the synclines, getting hotter toward their older rims (Fig. 10). This repartition becomes less clear on the eastern terminations of our two cross-sections. Hence, along the two cross-sections, when we could sample a large thickness of the Late Visean-Serpukhovian/Bashkirian infill from older to younger series, the distributions of temperatures follow the stratigraphical distribution. This "thermal stratification" mimics a thermal structure acquired through subsidence with a layered cake geometry. We can then examine if it more likely fits with compressional or extensional conditions.

In the case of compression and tectonic burial, given the W-verging nappes to the east (contractional or extensional nature is still debated) we could expect a decreasing burial load westward which at first-order seems in adequacy with the overall decrease of temperatures toward the west (Fig. 10). In this case, maturities were acquired during the Late Carboniferous contractional deformation and before the deposition of unconformable upper Pennsylvanian-Cisuralian rocks (Fig. 3). Anyway, this scenario implies that the Khenifra nappe was acquiring its maturities while it was thrusted and emplaced on top of the basin and we shall expect lower maturities on top of the nappe than within the basin, which is not the case. It also does not solve the overlapping Ordovician maturities on both sides of the basin.

In the case of syn-sedimentary burial, in an extensional context, we can explain the layer-cake thermal geometries with differential burial along the two cross-sections (see Fig. 10). Maturities were thus acquired during the latest stages of basin infill, and before the contractional deformations of the Late Carboniferous. The differential burial, with respect to the base of the basin could explain the E-W temperature variations, but implies a peculiar basement structure below the upper Visean series (Fig. 10) that cannot be verified without subsurface data. In addition, it should result in a complex model for the exhumation of the Ordovician basement at the contact with the Visean series, while the basin was deepening. In particular, any model shall explain the Ordovician/Lower Carboniferous temperatures relationships on both sides of the basin (Fig. 13). Based on this comparison, we favor the sedimentary burial hypothesis to account for the "thermal stratification". It is also more in agreement with our point (2).

The interpretations of our results for the southern AKB then make us consider a pre-Variscan maturity acquisition, during a single tectonic phase that saw both the metamorphic deformation of Ordovician and its exhumation likely in an extensional context together with the basin deepening that preserved a "simple" thermal stratification. Following this and given that the maturities of the Qasbat-Tadla basin were also acquired before the Mesozoic, we will consider that the two basins underwent a similar succession of tectono-metamorphic events, with maximum temperatures acquired before the Variscan stages, given their spatial connexion.

5.2.2. *Paleo-geotherms within the southern AKB*

To further confirm the tectonic context of the southern AKB development, we can try to get access to first order paleo-geotherms by using the temperatures distribution. The geotherm can indeed be associated with the tectonic context for basins developments as a fingerprint of it (Allen & Allen, 2005). A classical way to determine a geotherm requires a vertical sampling, *e.g.* in a well, along which we have a representative set of samples allowing the determination of the temperature at various depths. In our case this approach is not possible, and we will thus only access a "pseudo-vertical" section along erosional profiles *i.e.* "horizontal" sections on eroded anticlines or synclines flanks. By doing that, we accept some (not verifiable) hypotheses:

(1) Within the syncline/anticline flank, the initial thickness of the sedimentary piles before erosion were roughly equivalent between the syncline/anticline core and its flank.
(2) We also suppose that at the scale of km-scale structures like the ones we observe, the lateral thermal variations were not significant during the basin infill.

Knowing these limitations, the paleo-geotherms that will be derived are only first-order estimates that still should be used with caution. We will take two suitable places for these calculations, where we have enough geological information to constrain the sedimentary thickness that was sampled. These two places are the eastern flank of the Sidi Lamine sub-basin (cross-section A-A′, Fig. 10B) and the eastern flank of the syncline between the Tabaïnout massif and the Aït Mazel anticline core (cross-section B-B′, Fig. 10B). First, the Sidi Lamine sub-basin is an ideal place with a well-developed syncline-shape and well-dated core sediments, being younger than the flanks (Verset et al., 1988). Thus, from the core to the flanks of the structure, we cross a "pseudo-vertical" section along an erosional profile (cross-section A-A′, Fig. 10A). Going east, we obtain a ΔT ~120 °C that is realized within a sedimentary thickness estimated by Verset et al. (1988) to be within a 2.2–3 km range. This leads us to a paleo-geotherm of 40–55 °C.km^{-1}. It is worth noticing that the western flank of the sub-basin was not suitable for this evaluation since, following the cross-section A-A', the oldest Visean sediments are not outcropping to its western boundary, deeply buried along a fault separating it from the Ordovician basement.

For the second location, the eastern flank of the syncline structure shows an erosional profile that reveals a significant sedimentary thickness within upper Visean-Serpukhovian sediments, from younger to older ones. In this case, we obtain a ΔT ~90 °C for an estimated 1.3–1.7 km range for the sedimentary thickness (El Houicha, 1994). This gives us a 52–60 °C.km^{-1} paleo-geotherm.

Notwithstanding the fact that we have clear limitations in these calculations, we can notice that at first order the paleo-geotherms of both locations are consistent and overlapping, within the 40–60 °C range. These values are the first providing insights on the thermal structure of a lower Carboniferous basin in Morocco, since, given the interpretation of the RSCM data distribution, the RSCM temperatures do not represent a Variscan overprint on this poorly inverted basin. Let us notice that with such paleogeotherms, rough estimates of eroded sections on top of the Khenifra basin would indicate between 2 and 3.5 km of missing sedimentary section for the coldest recorded temperature (132 ± 18 °C, j4-2vis) up to between 4.3 and 6.5 km for the hottest recorded temperature (259 ± 10 °C, j3-10vis).

5.3. Contrasts between the southern AKB & Qasbat-Tadla basins

For the Qasbat-Tadla basin, we estimated maturities from Silurian samples, to be within 110–160 °C for KAT-1 well samples, at 0.7–0.8 km of present-day burial and within 150–175 °C for Boujad-105 samples, at 0.9–1 km of present-day burial. Within the southern AKB, we found equivalent maturities – within uncertainties – only within the youngest Serpukhovian/Bashkirian(?) samples with estimated values of 132 ± 18 °C or 143 ± 16 °C (samples j4-2vis and j5-8vis, respectively). These results consequently reveal in both basins the considered rocks, even though they have different stratigraphical ages, likely experienced similar thermal cooling from *ca.*~130–170 °C up to the surface (or close to the surface, for Qasbat-Tadla samples).

In Qasbat-Tadla basin, the limited thickness of the Silurian (~70 m in KAT-1, ~100 m in Boujad-105) enables to consider similar maturities for the whole (top) Ordovician-Silurian section. Now if we compare the Ordovician maturities of Qasbat-Tadla and southern AKB, the thermal difference between both basements ranges from 60 °C to as high as 170 °C (Table 1). Thus, this difference between basements of adjacent basins is likely inherited from contrasted lower Carboniferous crustal behaviors during the extensional sedimentary infills. Afterwards and given their geographical proximity, both basins can be expected to have undergone a similar erosional story from the onset of Variscan orogeny onwards. Moreover, the main erosional stage can be constrained in time. Indeed, field evidence shows unconformable and weakly deformed upper Pennsylvanian-Cisuralian deposition around Khenifra city (Fig. 3; El Wartiti et al., 1990) that sealed the more deformed lower Carboniferous rocks within the Khenifra basin. This proves that most of the deformation had already brought both the lower Carboniferous series of Khenifra basin and the top Ordovician-Silurian rocks of Qasbat-Tadla basin to the surface before being sealed below the unconformity of Late Pennsylvanian-Permian. Subsequent potential tectonic burial related to late Variscan stages is still possible but cannot be evidenced and Mesozoic-Cenozoic burial was not sufficient to reset the maturities acquired during the Early Carboniferous.

5.4. A new model for evolution the southern AKB

5.4.1. Previous evolution models

5.4.1.1. A tectonic point of view. Overall, one model dominates for the tectonic interpretation of the southern AKB, and in general the eastern MCM. This model claims that the main lower Carboniferous infill of the Khenifra basin occurred in an orogenic context, within which the Variscan deformation front had been migrating toward the west (Bouabdelli, 1989; Bouabdelli and Piqué, 1996; Ben Abbou, 2001; Michard et al., 2010). In this classical view, the pre-orogenic evolution of the southern AKB showed the succession of: (1) a Late Devonian extension, (2) a contractional Eovariscan event, at some point between the end of the Late Devonian and the Visean, (3) renewed subsidence due first to a general transgressive trend in the Visean but also with the progressive orogenic loading in relationship with the westward propagation of the Variscan front, up to the Namurian-Westphalian. This "classical" view has received a recent update in the Lahfid et al. (2019) study. The latter claim that an early orogenic "hot" belt was formed during the Tournaisian-Early Visean that was followed by a thermal subsidence stage allowing the upper Visean-Serpukhovian infill, up to the "real" beginning of the Variscan orogeny during the Late Carboniferous.

Another view of the evolution of the Khenifra basin and the eastern MCM puts forward the importance of purely extensional/transtensional events for its sedimentary infill, especially during Visean-Serpukhovian times (Allary et al., 1976; Huvelin, 1973; Faïk, 1988; Izart, 1991; El Houicha, 1994; Berkhli and Vachard, 2002; Vachard et al., 2006; Cózar et al., 2023b), alternating with contractional events (Eovariscan before, Variscan onset after). As a matter of fact, the Eovariscan event remains a contractional event for both types of models in most of the literature.

For these two types of models, the Eovariscan or sometimes "Meso-variscan" phase represents an early orogenic stage (Bouabdelli, 1989; El Houicha, 1994; Hoepffner et al., 2005, 2006; Lahfid et al., 2019; Accotto et al., 2020). This view has been criticized while studying the same time period in others places than the AKB. For instance, to account for the basement deformation in the Tamlelt (Houari, 2003) or theMidelt areas (Diot and Bouchez, 1989; see Fig. 1) authors proposed a fully extensional hypothesis that has been synthesized and extended by Chopin et al. (2023) and Leprêtre et al. (2024).

5.4.1.2. A thermal point of view. At least three studies addressed the thermal evolution of the Khenifra basin. Bouabdelli (1989, 1994) acquired illite crystallinity data along the basin (Fig. 14). Neqqazi et al. (2014) showed (with few samples) Conodont Alteration Index across the whole AKB (Fig. 2) with very altered samples. Yet, Neqqazi et al. (2014) data have been incorporated within our dataset but must be considered with caution (see Figs. 3 and 10). This data were converted into temperatures by Medina Varea (2018). Anyway, these data show a particularly high uncertainty so that they are difficult to tie with our own data.

Lahfid et al. (2019) realized an important RSCM sampling of Ordovician series of the Zaian in addition with few upper Visean-Serpukhovian samples (Fig. 3). They proposed that the acquisition of the maturities was realized during the Fammenian-Tournaisian (Eovariscan) compression. The main blocking point of their interpretation stems from a partial vision given they only sampled the western side of the system (like on Fig. 13A), which cannot hold for the eastern side at the same time. It is thus not consistent at the scale of the basin. A second issue is related to the way they estimated the paleo-geotherm. They suggested that the pre-Devonian layers kept a layered-cake thermal signature with the oldest being the hottest. But at the same time, they claim that the maximal temperatures were acquired after 50 % of Eovariscan shortening *i.e.* after that the layers were folded and thus had lost the simple layer-cake geometry (see their section on their Fig. 10). Moreover, they used a maximum temperature value for each layer that is a mean of the different samples of the same age that are spatially scattered on their sampling area (40 km × 60 km of extent). As such, and although their estimates are similar to our own, we consider that the paleo-geotherm of the Zaian Massif still remains poorly constrained.

In our study, we have estimated first order paleogeotherms within a 40–60 °C.km^{-1} range representative of the thermal conditions at the end of the basin infill (from Visean to Bashkirian at least). These represent high paleo-geothermal gradient values that can usually be found in the context of sedimentary burial within rifts, where these gradients can reach 50–60 to 90–100 °C.km^{-1} in hyperextended domains (Vacherat et al., 2014; Saspiturry et al., 2020; Célini et al., 2023). This is compatible with our conclusions on the analyses of the RSCM temperatures distribution and the field geology in the Khenifra basin (section 5.2.1). Together, this points toward a renewed view of the tectonic setting of the Khenifra basin that likely developed in an extensional context instead of a contractional one.

This conclusion cannot be directly applied to the context of development of the Qasbat-Tadla basin. Yet, given the important difference of maximum maturities between both basins, we think that both basins could represent a partial view of a more extended rift system within which the stretching factor were unequally distributed. This is a frequent observation within many rift systems (Saspiturry et al., 2020 with differently extended crustal domains). In our view, both basins belonged to a wide regional rifts system, within which the different behaviours could result from tectonic segmentation.

5.4.2. An updated extensional model

Any new model for the southern AKB should be able to explain: (i) the almost total lack of the Silurian-Devonian cover over most parts of

the area; (ii) the unconformity observed between the previously deformed Ordovician or older rocks and the overlying Visean-Serpukhovian rocks, containing re-sedimented metamorphosed Ordovician rocks; (iii) our new results indicating that acquisition time for maximum maturity is required to happen after the Late Visean-Bashkiran(?) infill and before the first Late Carboniferous Variscan stage; (iv) that the paleo-geotherm range was 40–60 °C.km^{-1}; (v) the differentiated distribution of the RSCM temperatures on both sides of the basin (Fig. 13).

We propose that the Khenifra basin followed a protracted extensional history since Middle-Late Devonian to the Bashkirian. The Paleozoic Morocco (Meseta & Anti-Atlas domains) were affected by important extensional events during the Devonian (Wendt, 1985; Michard et al., 2008; Frizon de Lamotte et al., 2013, Fig. 15) and it has also been remarked in the eastern MCM (Faïk, 1988; Bouabdelli et al., 1989), where Devonian layers were preserved. At the Late Devonian-Tournaisian transition and up to the middle Visean, an important magmatic activity has been revealed with the most recent dating works (Essaifi et al., 2003; Dostal et al., 2005; Marcoux et al., 2008; Ait Lahna et al., 2018; Delchini et al., 2018; Chopin et al., 2023). This magmatic activity affected both Mesetas and is mainly coeval to the development of deep turbiditic upper Visean basins (Leprêtre et al., 2024). Although direct evidence of this magmatic activity is very restricted within the Khenifra-Sidi Lamine sub-basins themselves (Birlea and Birlea, 1992; Ntarmouchant et al., 2002), its widespread occurrences could reveal an important thinning of the crust at the time (Late Devonian/Tournaisian to end of Visean). Within this context, we suggest that the extensional activity reached a peak within the Tournaisian to Early Visean interval (Fig. 15). The general lack of Tournaisian to Lower Visean deposits on the MCM (with the exception of the Sidi Bettache) or within both Mesetas in general (Marhoumi and Rauscher, 1983; Marhoumi and Rauscher, 1984; Huvelin & Mamet, 1988; Accotto et al., 2020; Cózar et al., 2020) leads us to consider that the area underwent a thermal uplift in extensional context that scalped a large part of Devonian to potential Tournaisian rift-related sediments (Fig. 15). This thermal uplift associated to important thinning was contemporaneous with the onset of the ductile Eovariscan deformation at depth, below the Silurian and the uppermost Ordovician shale layers that could have acted as good detachment layers. From Middle-Late Visean to the Serpukhovian/Bashkirian(?), the protracted extensional regime was thus responsible for the ductile to brittle exhumation of the metamorphosed basement rocks, subsequently embedded within the overlying unconformable sedimentary infill. This ductile to brittle exhumation could explain the foldings and rotations below the Eovariscan unconformity.

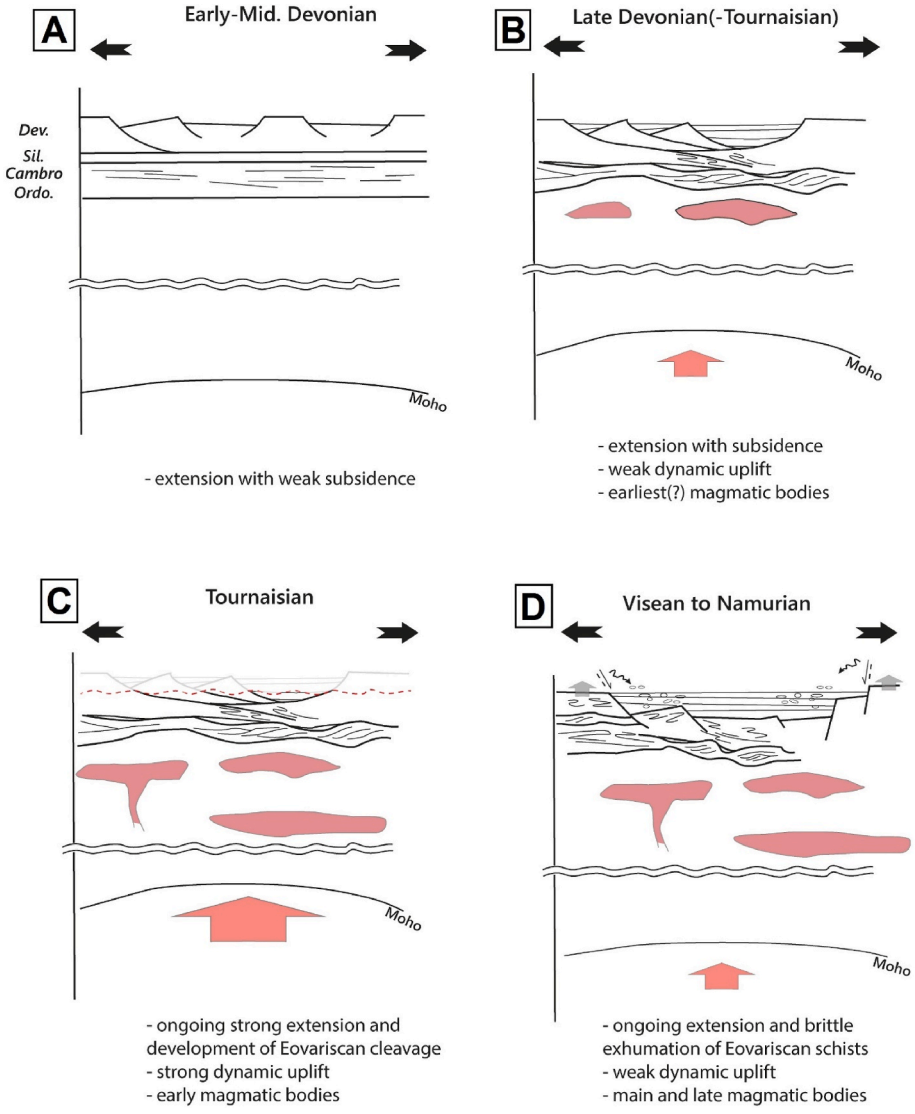

Fig. 15. Khenifra sub-basin model evolution from Devonian to Namurian times (A to D sketches). Pink colors indicate the intrusions of likely plutonic bodies during extension in association with the crust thinning. Red large arrows show the push of dynamic uplift through the mantle doming below the thinned crust.

The hypothesis of (1) a rapid burial under a thick lower-upper Visean to Bashkirian sedimentary cover, associated with (2) an overall hot crustal regime that witnessed pre-orogenic magmatic intrusions up to the Serpukhovian, enabled the record of hot syn-rift maximum temperatures between Early Visean and Bashkirian. Then, the observed situations on both sides of the basin represented the following situations: (1; Fig. 13B) either the syn-rift sediments have been directly in contact to the Ordovician deformed basement while the latter was exhumed at depth within the basin and acquired similar maximum temperatures during burial or (2; Fig. 13A) either the brittle deformation brought to the surface hot Ordovician basement (Zaian western boundary of the Khenifra basin) in contact with shallower upper Visean rocks not in direct contact with the basin floor and consequently colder, introducing the temperature jump we have witnessed with our data and the data of Lahfid et al. (2019).

5.5. *Consequences for the understanding of the north Moroccan Variscan segment*

The North Moroccan Variscan segment is an intraplate orogeny (Hoepffner et al., 2005, 2006; Michard et al., 2008, 2010, 2023). The recent developments on the highly deformed Jebilet and Rehamna massifs (Chopin et al., 2014; Wernert et al., 2016; Delchini et al., 2018) as well as Leprêtre et al.'s (2024) synthesis have accounted for a necessary pre-orogenic phase witnessing the development of lower Carboniferous rifts, based on structural, metamorphic and magmatic data together with datings. To a lesser extent, since the eastern MCM is less deformed, we demonstrated that the Khenifra basin behaved also as a rift from the Early Visean to the Bashkirian, incorporating within this explanatory scheme the Eovariscan deformation that was classically interpreted as a contractional event. The Early Visean– Serpukhovian/Bashkirian vision we now propose for North Morocco is that of a distributed and segmented rift system (Fig. 16A), in which the Jebilet and Rehamna represented very extended and hot rift segments with coeval magmatism (with T°C > 450–500 °C at low pressures *ca.* <4–6 kbars; Chopin et al., 2014; Wernert et al., 2016; Delchini et al., 2018) coexisting with less extended segments like the Khenifra one, showing intermediate maximum temperatures for its sedimentary infill (130–260 °C at P < 2 kbars) and other segments poorly affected from a thermal point of view, like the Qasbat-Tadla basin, whose basement shows the coldest temperatures (110–175 °C). This geological setting is in agreement with what Chopin et al. (2023) and Leprêtre et al. (2024) proposed. They consider that the Meseta domain was located at the tip of the Paleotethys oceanic propagator (Fig. 17), thus undergoing continental extension. The likeliness of this scenario could be confirmed by the recent evidence in internal Betics. There, Sánchez-Navas et al. (2024) found upper Cisuralian granulitic rocks showing a "too young" Barrovian metamorphism, with respect to the W. Europe Variscan belt. This could be related to the closure of the Paleotethys oceanic domain, significantly later than the main Devonian-Early Carboniferous Variscan collision in W Europe (Martínez Catalán et al., 2021). The scattered remnants of granulitic bodies sampled in the external autochthonous Tell and Rif belt Triassic diapirs (Midoun, 1989; Frizon de Lamotte, 1982) could also have witnessed this same event, since these rocks do not exist in any Variscan "autochthonous" outcrops of the NW African Variscan belt.

In addition to the geodynamic changes that our new proposal can induce, the presence of a wide hot rift system could be meaningful to understand the "intraplate" character of the Variscan segment in NW Africa. Indeed, the setting of these hot rift basins across the Meseta could have been able to efficiently weaken the lithosphere so that it localized the deformation during the subsequent inversion events. Thompson et al. (2001) or Schulmann et al. (2002), in the cases of thermally weakened lithosphere and its impact on thickening processes, showed that the rift thermal budget could be retained during *ca.* 30 to 40 Ma. Given our time lag of 20–25 Ma before the first inversion stages in north Morocco, this hypothesis is valid to understand how the Variscan deformation could be localized within this intraplate setting, and

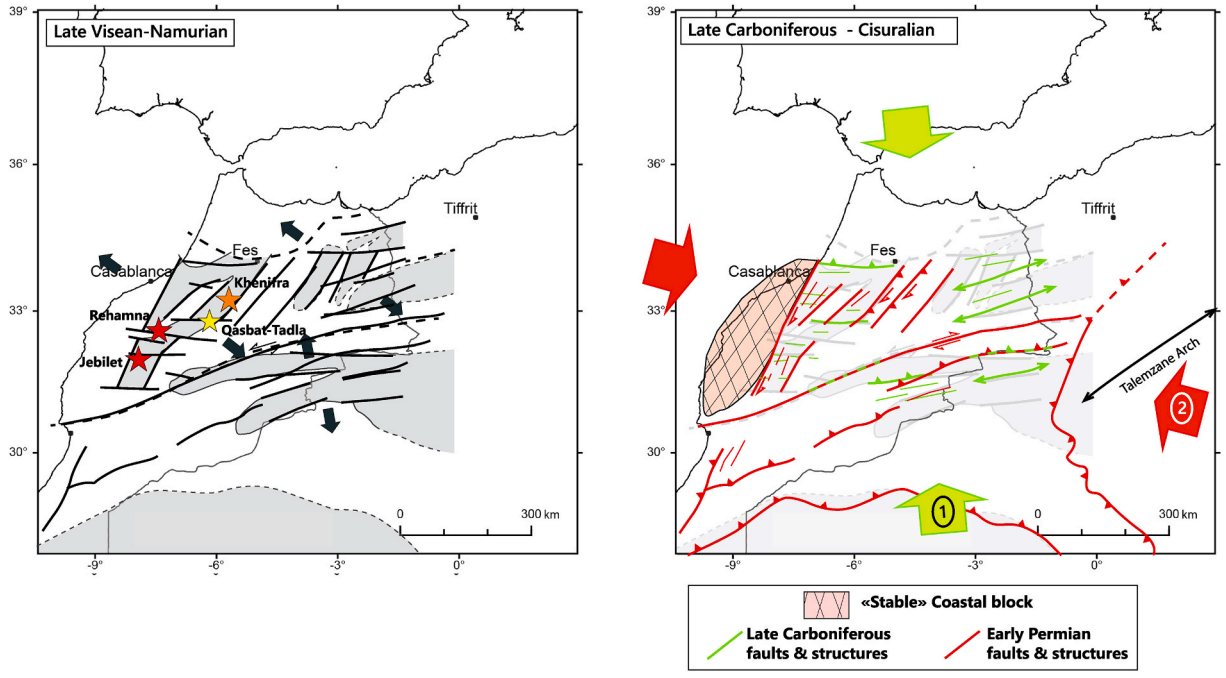

Fig. 16. Global evolution model for NW Morocco from the Early Carboniferous and Eovariscan times to Cisuralian times. (A) The left panel "Late Visean-Namurian" shows colored stars indicating lower Carboniferous basins (in grey) where thermal studies have been undertaken. Orange and yellow stars indicate the locations of the southern Azrou-Khenifra and Qasbat-Tadla basins, respectively. The red stars are showing the Rehamna and Jebilet massifs, where evidence of lower Carboniferous hot regimes were evidenced by Wernert et al. (2016) and Delchini (2018), respectively. (B) The right panel "Late Carboniferous-Cisuralian" shows the succession of compression phases with their main structures during this period with a first period (1) (in green) characterized – in present-day position – by N/S compression whereas a second period (2) (in red) is characterized by more E/W to ENE/WSW compression (following Chopin et al., 2014; Delchini et al., 2018).

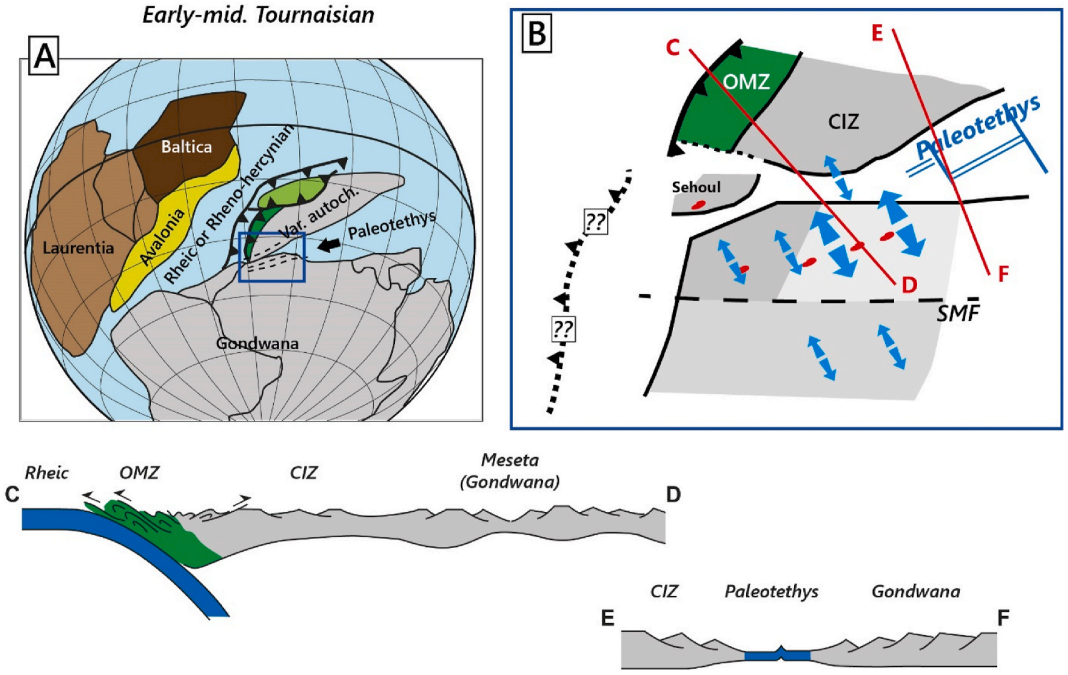

Fig. 17. Tournaisian paleogeographical reconstructions. (A) General paleogeography during early-middle Tournaisian (after Martínez Catalán et al., 2021) showing the different oceanic domains involved. (B) Focus on Morocco and the autochthonous Variscan terranes close to it (CIZ: Central Iberian Zone; OMZ: Ossa Morena Zone). The Paleotethys is propagating toward the SW in this present-day oriented map, inside Morocco, provoking crustal extension (blue arrows) and magmatism (red shapes). North of SMF are the two Meseta; South of the SMF is the Anti-Atlas and nearby Carboniferous basins. SMF: South Meseta Fault. Red lines show the traces of the two cross-section shown below. On the bottom part are two regional cross-sections showing the different tectonic regimes along this region at the time.

particularly well in the case of the western Meseta. The first inversion stage during the Late Carboniferous (Fig. 15B) produced the first main structures of the Variscan belt at the scale of both Meseta and Anti-Atlas domain, with E-W to WSW-ENE directions. A very important erosion took place between the Late Carboniferous stage and the beginning of the upper Pennsylvanian-Cisuralian as we demonstrated for the Khenifra and Qasbat-Tadla basins. Our results evidenced for both basins a ~130–170 °C of cooling at the time. The second, syn-to post-Cisuralian, stage then occurred with almost orthogonal deformation directions, setting mainly SW-NE to N-S structures.

6. Conclusion

The southern AKB and Qasbat-Tadla basins are two of the major lower Carboniferous basins of the NW African Variscides. For these two basins, we have proposed a thermal study leaning on RSCM temperatures and geochemistry of organic matter, respectively. We have identified that the southern AKB recorded high maximum temperatures within both the Ordovician basement and the lower Carboniferous infill. The Qasbat-Tadla basin is less known, given it is buried below Mesozoic-Cenozoic deposits, but organic matter maturity identifies a basin with lower thermal maturity. Together, these basins are considered to have undergone a similar history since the lower Carboniferous, in spite of their different thermal records.

The fact that the southern AKB stratigraphically recorded precisely the unconformities occurring between the Late Devonian and Serpukhovian is of great help to understand when the RSCM temperatures were acquired. The use of independent geological constraints enabled us to consider a late acquisition for these maximum temperatures, meaning during or at the end of the basin infill, between Visean to Serpukhovian/Bashkirian. If we are correct, it likely means that the Eovariscan deformation in the southern AKB is tightly related to the basin infills during this period, and not related to a compression event occurring earlier, before the Visean. In this case, it is forcing us to revise the meaning of the Eovariscan phase at the scale of the Meseta domain. We propose to make it the southwestern tip of the Paleotethys propagator. This propagator could have opened a hot rift system in northern Morocco, leading the way to a fragmentation re-used afterwards to focus the Variscan deformation in the former hot rift domains. The intraplate character of the NW African Variscan segment would thus be inherited from this initial rift phase, 20–30 of Ma before the rift inversion in Pennsylvanian-Cisuralian.

CRediT authorship contribution statement

R. Leprêtre: Writing – review & editing, Writing – original draft, Supervision, Investigation, Formal analysis, Data curation, Conceptualization. **M. El Houicha:** Writing – original draft, Validation, Investigation, Conceptualization. **A. Schito:** Writing – original draft, Methodology, Data curation, Conceptualization. **R. Ouchaou:** Investigation, Data curation. **F. Chopin:** Investigation. **P. Cózar:** Writing – original draft, Conceptualization.

Declaration of competing interest

The authors declare the following financial interests/personal relationships which may be considered as potential competing interests: Remi Lepretre reports administrative support was provided by CY Cergy Paris University. Remi Lepretre reports a relationship with CY Cergy Paris University that includes: employment. If there are other authors, they declare that they have no known competing financial interests or personal relationships that could have appeared to influence the work reported in this paper.

Data availability

Raw spectral data are shared in public digital repository.
Khenifra_Raman-all-spectra (Original data) (Figshare)

Acknowledgments

This work is the result of a field campaign realized in 2018 with R. Ouchaou as a master student, who benefited from a co-funding master scholarship from the IST in CY CergyParis Université. F. Chopin was supported by INSU,Tellus Syster funding for part of the work. The manuscript was improved thanks to comments of two anonymous reviewers.

Appendix A. Supplementary data

Supplementary data to this article can be found online at https://doi.org/10.1016/j.jafrearsci.2024.105406.

References

Accotto, C., Martínez Poyatos, D., Azor, A., Jabaloy-Sánchez, A., Talavera, C., Evans, N. J., Azdimousa, A., 2020. Tectonic evolution of the eastern Moroccan meseta: from late devonian forearc sedimentation to early carboniferous collision of an avalonian promontory. Tectonics 39. https://doi.org/10.1029/2019TC005976, 0–3.

Ait Lahna, A., Aarab, E.M., Youbi, N., Colombo Celso Gaeata, T., Bensalah, M., Boumehdi, M.A., Kei, S., Basei, M.A.S., 2018. The lalla tittaf formation (Rehamna, Morocco): paleoproterozoic or paleozoic age?. In: ICG2018-Joint Congress CAAWG9-AIC2-ICGAME3. Abstract Book. El Jadida, pp. 13–16.

Allary, A., Andrieux, J., Lavenu, A., Ribeyrolles, M., 1972. Les nappes hercyniennes de la Meseta sud-orientale (Maroc central). C. R. Acad. Sci. 274, 2284–2287. Paris.

Allary, A., Lavenu, A., Ribeyrolles, M., 1976. Étude tectonique et microtectonique d'un segment de chaîne hercynienne dans la partie sud-orientale du Maroc central. Notes Serv. géol. Maroc 261, 169.

Badra, L., Cailleux, Y., 1983. Le socle du Paléozoïque inférieur et le bassin viséen du Maroc Central sud-oriental. PICG, Livret-guide, excursion B1 n°27, Rabat.

Baidder, L., Michard, A., Soulaimani, A., Fekkak, A., Eddebbi, A., Rjimati, E.C., Raddi, Y., 2016. Fold interference pattern in thick-skinned tectonics; a case study from the external Variscan belt of Eastern Anti-Atlas, Morocco. J. Afr. Earth Sci. 119, 204–225. https://doi.org/10.1016/j.jafrearsci.2016.04.003.

Ballèvre, M., Martínez Catalán, J.R., López-Carmona, A., Pitra, P., Abati, J., Fernández, R.D., Ducassou, C., Arenas, R., Bosse, V., Castiñeiras, P., Fernández-Suárez, J., Gómez Barreiro, J., Paquette, J.-L., Peucat, J.-J., Poujol, M., Ruffet, G., Sánchez Martínez, S., 2014. Correlation of the nappe stack in the Ibero-Armorican arc across the Bay of Biscay: a joint French–Spanish project. Geol. Soc. London, Spec. Publ. 405, 77–113. https://doi.org/10.1144/SP405.13.

Barbero, L., Jabaloy, A., Gómez-Ortiz, D., Pérez-Peña, J.V., Rodríguez-Peces, M.J., Tejero, R., Estupiñan, J., Azdimousa, A., Vázquez, M., Asebriy, L., 2011. Evidence for surface uplift of the Atlas Mountains and the surrounding peripheral plateaux: combining apatite fission-track results and geomorphic indicators in the Western Moroccan Meseta (coastal Variscan Paleozoic basement). Tectonophysics 502 (1–2), 90–104.

Beauchamp, J., Izart, A., 1987. Early Carboniferous basins of the Atlas-Meseta domain (Morocco): sedimentary model and geodynamic evolution. Geology 15 (9), 797–800.

Becker, R.T., El Hassani, A., Aboussalam, Z.S., 2020. Devonian to lower carboniferous stratigraphy and facies of the western Moroccan meseta : implications for palaeogeography and structural interpretation. Front. Sci.Eng. 10 (1).

Ben Abbou, M., 2001. Dynamique des bassins d'avant-pays carbonifères: Signatures tectoniques, sédimentaires et magmatique de l'évolution de la chaîne hercynienne du Maroc central septentrional. In: Implications sur le modèle géodynamique de la chaîne hercynienne. Univ. Cadi Ayyad, Marrakech, Morocco, p. 312. PhD thesis.

Berkhli, M., Vachard, D., 2002. Le Carbonifère du Maroc central : les formations de Migoumess, de Tirhela et d'Idmarrach. Lithologie, biostratigraphie et conséquences géodynamiques. Compt. Rendus Geosci. 334, 67–72. https://doi.org/10.1016/S1631-0713(02)01699-1.

Beyssac, O., Goffé, B., Chopin, C., Rouzaud, J.N., 2002. Raman spectra of carbonaceous material in metasediments: a new geothermometer. J. Metamorph. Geol. 20 (9), 859–871.

Birlea, V., Birlea, L., 1992. Volcanisme viséen supérieur dans le Bassin de Sidi Lamine, Maroc hercynien central. Notes Mém. Serv. Géol, Maroc, n°366 165–175.

Boote, D.R.D., Clark-Lowes, D.D., Traut, M.W., 1998. Palaeozoic petroleum systems of North Africa. Geol. Soc. Spec. Publ. 132, 7–68. https://doi.org/10.1144/GSL.SP.1998.132.01.02.

Bouabdelli, M., 1982. Stratigraphie et évolution structurale du Paléozoïque d'Azrou (NE du Maroc Central). Univ., Strasbourg. PhD thesis.

Bouabdelli, M., 1989. Tectonique et sédimentation dans un bassin orogénique: le sillon viséen d'Azrou-Khenifra (Est du Massif Hercynien Central du Maroc). Institut de géologie, Strasbourg.

Bouabdelli, M., 1994. Tectonique de l'Est du Massif hercynien central (zone d'Azrou-Khénifra). Bull. l'Institut Sci. Rabat 145–168.

Bouabdelli, M., Piqué, A., 1996. Du bassin sur décrochement au bassin d'avant-pays: Dynamique du bassin d'Azrou-Khénifra (Maroc hercynien central). J. Afr. Earth Sci. 23, 213–224. https://doi.org/10.1016/S0899-5362(96)00063-2.

Broutin, J., Aassoumi, H., El Wartiti, M., Freytet, P., Kerp, H., Quesada, C., 1998. The permian basins of tiddas, Bou achouch and Khenifra (central Morocco). Biostratigraphic and palaeophytogeographic implications. Mem. Mus. Natl. Hist. Nat. 179, 257–278.

Burkhard, M., Caritg, S., Helg, U., Robert-Charrue, C., Soulaimani, A., 2006. Tectonics of the anti-atlas of Morocco. Compt. Rendus Geosci. 338, 11–24. https://doi.org/10.1016/j.crte.2005.11.012.

Célini, N., Mouthereau, F., Lahfid, A., Gout, C., Callot, J.P., 2023. Rift thermal inheritance in the SW Alps (France): insights from RSCM thermometry and 1D thermal numerical modelling. Solid Earth 14 (1), 1–16.

Charrière, A., 1990. Héritage hercynien et évolution géodynamique alpine d'une chaîne intracontinentale: Le Moyen-Atlas au SE de Fes (Maroc). PhD, Toulouse.

Chopin, F., Corsini, M., Schulmann, K., El Houicha, M., Ghienne, J.-F., Edel, J.-B., 2014. Tectonic evolution of the Rehamna metamorphic dome (Morocco) in the context of the Alleghanian-Variscan orogeny. Tectonics 33, 1154–1177. https://doi.org/10.1002/2014TC003539.

Chopin, F., Leprêtre, R., El Houicha, M., Tabaud, A.S., Schulmann, K., Míková, J., Barbarand, J., Chebli, R., 2023. U–Pb geochronology of Variscan granitoids from the Moroccan Meseta (Northwest Africa): tectonic implications. Gondwana Res. 117, 274–294. https://doi.org/10.1016/j.gr.2023.02.004.

Corsini, M., 1988. Relation entre la marge du bassin cambrien et la cinématique hercynienne de la Meseta occidentale du Maroc: un exemple de l'influence de l'héritage tectono-sédimentaire dans une chaîne intracontinentale. Université de droit, d'économie et des sciences-Aix-Marseille III. France.

Cózar, P., Vachard, D., Izart, A., Said, I., Somerville, I., Rodríguez, S., Coronado, I., El Houicha, M., Ouarhache, D., 2020. Lower-middle Viséan transgressive carbonates in Morocco: palaeobiogeographic insights. J. Afr. Earth Sci. 168 https://doi.org/10.1016/j.jafrearsci.2020.103850.

Cózar, P., Vachard, D., Somerville, I.D., 2023a. Foraminifers and calcareous algae in Brigantian rocks as guides for the recognition of the Viséan-Serpukhovian boundary interval of Morocco. Comptes Rendus Palevol.

Cózar, P., Somerville, I.D., Rodríguez, S., El Houicha, M., Vachard, D., García-Frank, A., Coronado, I., Izart, A., Said, I., 2023b. Contrasting reef patterns during the evolution of the carboniferous Azrou-Khenifra basin (Moroccan Meseta). Facies 69 (1), 1.

Delchini, S., Lahfid, A., Lacroix, B., Baudin, T., Hoepffner, C., Guerrot, C., Lach, P., Saddiqi, O., Ramboz, C., 2018. The geological evolution of the variscan jebilet massif, Morocco, inferred from new structural and geochronological analyses. Tectonics 37, 4470–4493. https://doi.org/10.1029/2018TC005002.

Diot, H., Bouchez, J.L., 1989. Les granitoïdes hercyniens de la Haute-Moulouya (Maroc): leur structure primaire déduite de l'ASM. Indications sur leur mise en place. Bull. Soc. Geol. Fr. 5, 705–716. https://doi.org/10.2113/gssgfbull.v.4.705.

Domeier, M., Font, E., Youbi, N., Davies, J., Nemkin, S., Van der Voo, R., Perrot, M., Ben Abbou, M., Boumehdi, M.A., Torsvik, T.H., 2021. On the Early Permian shape of Pangea from paleomagnetism at its core. Gondwana Res. 90, 171–198. https://doi.org/10.1016/j.gr.2020.11.005.

Dostal, J., Keppie, J.D., Hamilton, M.A., Aarab, E.M., Lefort, J.P., Murphy, J.B., 2005. Crustal xenoliths in Triassic lamprophyre dykes in western Morocco: tectonic implications for the Rheic Ocean suture. Geol. Mag. 142, 159–172. https://doi.org/10.1017/S0016756805000440.

Drot, J., Morin, P., 1962. Première preuve paléontologique de l'âge ordovicien des schistes d'Asfar (Anticlinorium de Kasba-Tadla-Azrou, Maroc central). CR Acad. Sci. Paris 254, 1837–1839.

Edel, J.B., Schulmann, K., Lexa, O., Lardeaux, J.M., 2018. Late Palaeozoic palaeomagnetic and tectonic constraints for amalgamation of Pangea supercontinent in the European Variscan belt. Earth Sci. Rev. 177, 589–612. https://doi.org/10.1016/j.earscirev.2017.12.007.

El Houicha, M., 1994. Dynamique d'un bassin orogénique et processus gravitaires syn- à tardi-sédimentaires : le sillon viséo-namurien de Khénifra (SE du Massif hercynien central du Maroc). Université Cadi Ayyad, Marrakech.

El Houicha, M., Chopin, F., Tessitore, L., Ghienne, J.-F., Jouhari, A., Vanderbroucke, T., Schulmann, K., 2018. Revisiting the middle -late visean unconformity in the SE Moroccan massif central: new data and perspectives. In: ICG, Joint Congress-CAAWG9-AIC2-ICGAME3, 20–24 March, El Jadida, Abstr. vol., 87–89.

El Wartiti, M., Broutin, J., Freytet, P., Larhrib, M., Toutin-Morin, N., 1990. Continental deposits in Permian basins of the Mesetian Morocco, geodynamic history. J. Afr. Earth Sci. 10 (1–2), 361–368.

Er-Raïoui, H., Bouabdelli, M., Bélayouni, H., Chellai, H., 2001. Géodynamique et évolution thermique de la matière organique : exemple du bassin de Qasbat-Tadla, Maroc central. J. Afr. Earth Sci. 32 (4), 605–618.

Er-Raji, A., 1997. Analyse des terrains carbonifères de la région de Jerada (Maroc oriental) à partir des données de terrain, de forages et de sismique réflexion : stratigraphie, pétrographie du charbon, analyse structurale et modélisation cinématique de la déformation tardi-hercynienne. Université Mohammed-V, Rabat.

Espitalié, J., Madec, M., Tissot, B., 1980. Role of mineral matrix in kerogen pyrolysis: influence on petroleum generation and migration. AAPG (Am. Assoc. Pet. Geol.) Bull. 64 (1), 59–66.

Essaifi, A., Potrel, A., Capdevila, R., Lagarde, J.-L., 2003. Datation U-Pb : Âge de mise en place du magmatisme bimodal des Jebilet centrales (chaîne Varisque, Maroc). Implications géodynamiques. Comptes Rendus - Geosci. 335, 193–203. https://doi.org/10.1016/S1631-0713(03)00030-0.

Faïk, F., 1988. La paléozoïque de la région de Mrirt (Est du Maroc Central) : Evolution stratigraphique et structurale. Université Toulouse III.

Franke, W., Cocks, L.R.M., Torsvik, T.H., 2017. The Palaeozoic Variscan oceans revisited. Gondwana Res. 48, 257–284. https://doi.org/10.1016/j.gr.2017.03.005.

Frizon de Lamotte, D., 1982. Contribution à l'étude de l'évolution structurale du Rif oriental. Notes & Mém. Serv. géol. Maroc 314, 239–309.

Frizon de Lamotte, D., Tavakoli-Shirazi, S., Leturmy, P., Averbuch, O., Mouchot, N., Raulin, C., Leparmentier, F., Blanpied, C., Ringenbach, J.-C., 2013. Evidence for Late

Devonian vertical movements and extensional deformation in northern Africa and Arabia: integration in the geodynamics of the Devonian world. Tectonics 32, 107–122. https://doi.org/10.1002/tect.20007.
Ghorbal, B., Bertotti, G., Foeken, J., Andriessen, P., 2008. Unexpected Jurassic to Neogene vertical movements in 'stable'parts of NW Africa revealed by low temperature geochronology. Terra. Nova 20 (5), 355–363.
Hatcher, R.D., Tollo, R.P., Bartholomew, M.J., Hibbard, J.P., Karabinos, P.M., 2010. The Appalachian orogen: a brief summary. From Rodinia to Pangea: The Lithotectonic Record of the Appalachian Region: Geol. Soc. Am. Memoir 206, 1–19.
Henry, D.G., Jarvis, I., Gillmore, G., Stephenson, M., 2019. Raman spectroscopy as a tool to determine the thermal maturity of organic matter: application to sedimentary, metamorphic and structural geology. Earth Sci. Rev. 198, 102936.
Hmich, D., Schneider, J.W., Saber, H., Voigt, S., El Wartiti, M., 2006. New continental Carboniferous and Permian faunas of Morocco: implications for biostratigraphy, palaeobiogeography and palaeoclimate. Geol. Soc. London, Special Publ. 265 (1), 297–324.
Hoepffner, C., 1974. Contribution à la géologie structurale des Rehamna (Meseta marocaine méridionale), Le matériel paléozoïque et son évolution hercynienne dans l'est du massif. Université Louis Pasteur, Strasbourg.
Hoepffner, C., 1978. Le massif paléozoique du Tazekka (Maroc) ; analyse des déformations liées à un linéament tectonique. Sci. Géologiques. Bull. 31, 33–44. https://doi.org/10.3406/sgeol.1978.1531.
Hoepffner, C., 1987. La tectonique hercynienne dans l'Est du Maroc. Univ. Louis Pasteur, Strasbourg.
Hoepffner, C., Soulaimani, A., Piqué, A., 2005. The Moroccan hercynides. J. Afr. Earth Sci. 43, 144–165. https://doi.org/10.1016/j.jafrearsci.2005.09.002.
Hoepffner, C., Houari, M.R., Bouabdelli, M., 2006. Tectonics of the north african Variscides (Morocco, western Algeria): an outline. Compt. Rendus Geosci. 338, 25–40. https://doi.org/10.1016/j.crte.2005.11.003.
Houari, M.R., 2003. Etude structurale de la boutonnière paléozoïque de Tamlelt (Haut Atlas oriental) : sa place dans la chaîne hercynienne du Maroc. Université Mohammed 1er, Oujda.
Houari, M.R., Hoepffner, C., 2003. Late carboniferous dextral wrench-dominated transpression along the north african craton margin (eastern high-atlas, Morocco). J. Afr. Earth Sci. 37, 11–24. https://doi.org/10.1016/S0899-5362(03)00085-X.
Huvelin, P., 1973. Déformations hercyniennes précoces dans la région comprise entre Azrou, Aguelmous et Khénifra (Massif hercynien central). Notes Serv. Geol. Maroc 34 (254), 93–107.
Huvelin, P., 1977. Etude géologique et gîtologique du Massif hercynien des Jebilet (Maroc occidental). Notes Mém Serv Géol Maroc 232 bis 1–307.
Huvelin, P., Mamet, B., 1997. Transgressions, faulting and redeposition phenomenon during the Visean in the Khenifra area, western Moroccan Meseta. J. Afr. Earth Sci. 25 (3), 383–389. https://doi.org/10.1016/S0899-5362(97)00111-5.
Izart, A., 1990. Dynamique des corps sédimentaires clastiques dans les bassins carbonifères de la meseta marocaine. In: Thèse D'habilitation. Univ. Bourgogne, France.
Izart, A., 1991. Les bassins carbonifères de la Meseta marocaine, étude sédimentologique et approche du contexte structural. Part de la tectonique et de l'eustatisme. Geol. Mediterr. 18 (1), 61–72.
Jabour, H., Nakayama, K., 1988. Basin modeling of Tadla basin, Morocco, for hydrocarbon potential. AAPG Bull. 72 (9), 1059–1073.
Katz, B.J., 1983. Limitations of 'Rock-Eval'pyrolysis for typing organic matter. Org. Geochem. 4 (3–4), 195–199.
Kharbouch, F., 1994. Les laves dévono-dinantiennes de la Meseta marocaine : étude pétro-géochimique et implications géodynamiques. In: Université de Bretagne Occidentale. France.
Lahfid, A., Beyssac, O., Deville, E., Negro, F., Chopin, C., Goffé, B., 2010. Evolution of the Raman spectrum of carbonaceous material in low-grade metasediments of the Glarus Alps (Switzerland). Terra. Nova 22 (5), 354–360.
Lahfid, A., Baidder, L., Ouanaimi, H., Soulaimani, A., Hoepffner, C., Farah, A., Saddiqi, O., Michard, A., 2019. From extension to compression: high geothermal gradient during the earliest Variscan phase of the Moroccan Meseta; a first structural and RSCM thermometric study. Eur. J. Mineral 31, 695–713. https://doi.org/10.1127/ejm/2019/0031-2882.
Leprêtre, R., Chopin, F., El Houicha, M., Tabaud, A.-S., Schulmann, K., Ghienne, J.-F., Villeneuve, M., Aghzer, A.M., Gärtner, A., Guillou, O., Youbi, N., El Archi, A., 2024. The Variscides in the NW corner of Africa. In: Hamimi (Ed.), The Geology of North Africa Regional. Geology Reviews. Springer, Cham. https://doi.org/10.1007/978-3-031-48299-1_6.
Letsch, D., El Houicha, M., von Quadt, A., Winkler, W., 2018. A missing link in the peri-Gondwanan terrane collage: the Precambrian basement of the Moroccan Meseta and its lower Paleozoic cover. Can. J. Earth Sci. 55, 33–51. https://doi.org/10.1139/cjes-2017-0086.
Lünsdorf, N.K., 2016. Raman spectroscopy of dispersed vitrinite—methodical aspects and correlation with reflectance. Int. J. Coal Geol. 153, 75–86.
Lünsdorf, N.K., Dunkl, I., Schmidt, B.C., Rantitsch, G., von Eynatten, H., 2017. Towards a higher comparability of geothermometric data obtained by Raman spectroscopy of carbonaceous material. Part 2: a revised geothermometer. Geostand. Geoanal. Res. 41 (4), 593–612.
Marcoux, E., Belkabir, A., Gibson, H.L., Lentz, D., Ruffet, G., 2008. Draa Sfar, Morocco: a Visean (331 Ma) pyrrhotite-rich, polymetallic volcanogenic massive sulphide deposit in a Hercynian sediment-dominant terrane. Ore Geol. Rev. 33, 307–328. https://doi.org/10.1016/j.oregeorev.2007.03.004.
Marhoumi, M.R., Hoepffner, C., Doubinger, J., Rauscher, R., 1983. Données nouvelles sur l'histoire hercynienne de la Meseta orientale au Maroc: l'âge dévonien des schistes de Debdou et du Mekam. Comptes-rendus des séances l'Académie des Sci. Série 2 (297), 69–72.
Marhoumi, R., Rauscher, R., 1984. Un plancton dévonien de la meseta orientale au maroc. Rev. Palaeobot. Palynol. 43, 237–253. https://doi.org/10.1016/0034-6667(84)90035-6.
Medina Varea, P., 2018. Conodontos del Carbonífero de la Meseta Central y de la Cuenca de Tindouf (Marruecos).
Michard, A., 1982. Le massif paléozoïque des Rehamna (Maroc). Stratigraphie, tectonique et pétrogenèse d'un segment de la chaine varisque. Notes Mém. Serv. Géol. Maroc 303, 1–180.
Michard, A., Hoepffner, C., Soulaimani, A., Baidder, L., 2008. The variscan belt. Lect. Notes Earth Sci. 116, 65–132. https://doi.org/10.1007/978-3-540-77076-3_3.
Michard, A., Soulaimani, A., Hoepffner, C., Ouanaimi, H., Baidder, L., Rjimati, E.C., Saddiqi, O., 2010. The South-western branch of the variscan belt: evidence from Morocco. Tectonophysics. https://doi.org/10.1016/j.tecto.2010.05.021.
Michard, A., Lahfid, A., Baidder, L., Hoepffner, C., Ouanaimi, H., Soulaimani, A., Farah, A., Saddiqi, O., 2022. New structural and RSCM thermometric data from the variscan orogen of Morocco: insight into the extension-to-compression transition. In: Meghraoui, M., et al. (Eds.), Advances in Geophysics, Tectonics and Petroleum Geosciences. CAJG 2019. Advances in Science, Technology & Innovation. Springer, Cham, pp. 599–604. https://doi.org/10.1007/978-3-030-73026-0_133.
Michard, A., Driouch, Y., Kuiper, Y.D., Caby, R., Farah, A., Ouanaimi, H., Soulaimani, A., Chabou, M.C., Saddiqi, O., 2023. The variscan belts of North-west Africa: an african legacy to the wilson cycle concept. J. Afr. Earth Sci. 208, 105042 https://doi.org/10.1016/j.jafrearsci.2023.105042.
Midoun, M., 1989. Etude du trias d'oranie (Algerie) et de ses relations avec le socle polymetamorphique: implications geodynamiques regionales. Univ. Orléans. PhD thesis.
Morin, P., 1973. L'accident de Bsabis-Tazekka, un linéament majeur de la tectonique hercynienne du Maroc (Ouest de Taza). CR somm. Soc. géol. Fr 2, 64–67.
Mrini, Z., Rafi, A., Duthou, J.L., Vidal, P., 1992. Chronologie Rb-Sr des granitoides hercyniens du Maroc; consequences. Bull. la Société Géologique Fr 163, 281–291.
Muirhead, D.K., Bond, C.E., Watkins, H., Butler, R.W.H., Schito, A., Crawford, Z., Marpino, A., 2020. Raman spectroscopy: an effective thermal marker in low temperature carbonaceous fold–thrust belts. Geological Society 490 (1), 135–151. London, Special Publications.
Neqqazi, A., Raji, M., Benfrika, E., 2014. Colour Alteration index (CAI) of Visean conodonts from the Azrou-Khénifra basin (Moroccan meseta). Bulletin de l'Institut Scientifique, Rabat, Section Sciences de la Terre 36, 13–18.
Nielsen, S.B., Clausen, O.R., Mcgregor, E., 2017. basin%Ro: a vitrinite reflectance model derived from basin and laboratory data. Basin Res. 29, 515–536. https://doi.org/10.1111/bre.12160.
Ntarmouchant, A., 2003. Le magmatisme associé à l'orogenèse du Maroc varisque: exemple du magmatisme du bassin méridional d'Azrou-Khénifra (Est du Maroc hercynien central). PhD thesis. Université de Fès, Maroc.
Ntarmouchant, A., Ribeiro, M.L., Moreira, M.E., Ramos, J.F., 2002. Le magmatisme terminal de la chaîne hercynienne: signification géodynamique d'une association magmatique identifiée dans le carbonifère terminal du Massif hercynien Central Marocain. Comunicacoes do Inst. Geol. Min. 89, 239–248.
Ouabid, M., Ouali, H., Garrido, C.J., Acosta-Vigil, A., Román-Alpiste, M.J., Dautria, J.M., Marchesi, C., Hidas, K., 2017. Neoproterozoic granitoids in the basement of the Moroccan central meseta: correlation with the Anti-Atlas at the NW paleo-margin of Gondwana. Precambrian Res. 299, 34–57. https://doi.org/10.1016/j.precamres.2017.07.007.
Ouabid, M., Garrido, C.J., 2023. Widespread Cadomian–Pan-African Ediacaran magmatism across the Moroccan meseta: Implication for the geodynamic evolution of the NW Gondwana margin. Precambrian Res. 387, 106992 https://doi.org/10.1016/j.precamres.2023.106992.
Petersen, H.I., Schovsbo, N.H., Nielsen, A.T., 2013. Reflectance measurements of zooclasts and solid bitumen in Lower Paleozoic shales, southern Scandinavia: correlation to vitrinite reflectance. Int. J. Coal Geol. 114, 1–18.
Piqué, A., Michard, A., 1989. Moroccan Hercynides: a synopsis. The Paleozoic sedimentary and tectonic evolution at the northern margin of West Africa. Am. J. Sci. 289, 286–330. https://doi.org/10.2475/ajs.289.3.286.
Roddaz, M., Brusset, S., Soula, J.-C., Béziat, D., Ben Abbou, M., Debat, P., Driouch, Y., Christophoul, F., Ntarmouchant, A., Déramond, J., 2002. Foreland basin magmatism in the Western Moroccan Meseta and geodynamic inferences. Tectonics 21, 1043. https://doi.org/10.1029/2001TC901029.
Rodríguez, S., Somerville, I.D., Cózar, P., Sanz-López, J., Coronado, I., González, F., Said, I., El Houicha, M., 2020. A new early Visean coral assemblage from Azrou-Khenifra Basin, central Morocco and palaeobiogeographic implications. J. Palaeogeogr. 9 https://doi.org/10.1186/s42501-019-0051-5.
Saddiqi, O., El Haimer, F.Z., Michard, A., Barbarand, J., Ruiz, G.M.H., Mansour, E.M., Leturmy, P., Frizon de Lamotte, D., 2009. Apatite fission-track analyses on basement granites from south-western Meseta, Morocco: Paleogeographic implications and interpretation of AFT age discrepancies. Tectonophysics 475 (1), 29–37.
Sánchez-Navas, A., Martín-Algarra, A., Blanco-Quintero, I., Garcia-Casco, A., 2024. Pre-Alpine prograde evolution of the Upper Alpujarride (Betic-Rif belt) reveals a Paleotethys-related collision. Int. Geol. Rev. 66 (1), 405–438.
Saspiturry, N., Lahfid, A., Baudin, T., Guillou-Frottier, L., Razin, P., Issautier, B., Le Bayon, B., Serrano, O., Lagabrielle, Y., Corre, B., 2020. Paleogeothermal gradients across an inverted hyperextended rift system: example of the Mauléon Fossil rift (western Pyrenees). Tectonics 39 (10), e2020TC006206.
Schito, A., Romano, C., Corrado, S., Grigo, D., Poe, B., 2017. Diagenetic thermal evolution of organic matter by Raman spectroscopy. Org. Geochem. 106, 57–67.

Schito, A., Spina, A., Corrado, S., Cirilli, S., Romano, C., 2019. Comparing optical and Raman spectroscopic investigations of phytoclasts and sporomorphs for thermal maturity assessment: the case study of Hettangian continental facies in the Holy cross Mts.(central Poland). Mar. Petrol. Geol. 104, 331–345.

Schito, A., Muirhead, D.K., Parnell, J., 2023. Towards a kerogen-to-graphite kinetic model by means of Raman spectroscopy. Earth Sci. Rev. 237, 104292.

Schmidt, J.S., Hinrichs, R., Araujo, C.V., 2017. Maturity estimation of phytoclasts in strew mounts by micro-Raman spectroscopy. Int. J. Coal Geol. 173, 1–8.

Schulmann, K., Schaltegger, U., Jezek, J., Thompson, A.B., Edel, J.B., 2002. Rapid burial and exhumation during orogeny: thickening and synconvergent exhumation of thermally weakened and thinned crust (Variscan orogen in Western Europe). Am. J. Sci. 302 (10), 856–879.

Senftle, J.T., Landis, C.R., 1991. Vitrinite reflectance as a tool to assess thermal maturity. Geochem. Methods Explor. (Chapter 12).

Simancas, J.F., Azor, A., Martínez-Poyatos, D., Tahiri, A., El Hadi, H., González-Lodeiro, F., Pérez-Estaún, A., Carbonell, R., 2009. Tectonic relationships of southwest Iberia with the allochthons of Northwest Iberia and the Moroccan Variscides. Compt. Rendus Geosci. 341, 103–113. https://doi.org/10.1016/j.crte.2008.11.003.

Sweeney, J.J., Burnham, A.K., 1990. Evaluation of a simple model of vitrinite reflectance based on chemical kinetics. AAPG Bull. 74 (10), 1559–1570.

Tahiri, A., Montero, P., El Hadi, H., Martínez Poyatos, D., Azor, A., Bea, F., Simancas, J. F., González Lodeiro, F., 2010. Geochronological data on the Rabat-Tiflet granitoids: their bearing on the tectonics of the Moroccan Variscides. J. Afr. Earth Sci. 57, 1–13. https://doi.org/10.1016/j.jafrearsci.2009.07.005.

Thompson, A.B., Schulmann, K., Jezek, J., Tolar, V., 2001. Thermally softened continental extensional zones (arcs and rifts) as precursors to thickened orogenic belts. Tectonophysics 332 (1–2), 115–141.

Torbi, A., 1996. Stratigraphie et évolution structurale paléozoïque d'un segment de la Meseta orientale marocaine (Monts du Sud-Est d'Oujda): Rôle des décrochements dans la formation de l'olistostrome intraviséen et le plutonisme tardi-hercynien. J. Afr. Earth Sci. 22, 549–563. https://doi.org/10.1016/0899-5362(96)00036-X.

Tuinstra, F., Koenig, J.L., 1970. Raman spectrum of graphite. J. Chem. Phys. 53 (3), 1126–1130.

Vachard, D., Orberger, B., Rividi, N., Pille, L., Berkhli, M., 2006. New late Asbian/early Brigantian (late Visean, Mississippian) dates in the Mouchenkour formation (central Morocco): palaeogeographical consequences. Comptes Rendus Palevol 5, 769–777. https://doi.org/10.1016/j.crpv.2006.03.004.

Vacherat, A., Mouthereau, F., Pik, R., Bernet, M., Gautheron, C., Masini, E., Le Pourhiet, L., Tibari, B., Lahfid, A., 2014. Thermal imprint of rift-related processes in orogens as recorded in the Pyrenees. Earth Planet Sci. Lett. 408, 296–306.

Verset, Y., 1985. Geological map of the Qasbat-Tadla. Notes Mém. Serv. géol. Maroc 340.

Verset, Y., Chartry, G., Nataf, M., 1988. Carte géologique du Maroc au 1/100 000 feuille Qasbat-Tadla, Mémoire explicatif. Notes Mém. Serv. géol. Maroc 340bis 132pp.

Wendt, J., 1985. Disintegration of the continental margin of northwestern Gondwana: late Devonian of the eastern Anti- Atlas (Morocco). Geology 13, 815–818. https://doi.org/10.1130/0091-7613(1985)13<815:DOTCMO>2.0.CO;2.

Wernert, P., Schulmann, K., Chopin, F., Štípská, P., Bosch, D., El Houicha, M., 2016. Tectonometamorphic evolution of an intracontinental orogeny inferred from P–T–t–d paths of the metapelites from the Rehamna massif (Morocco). J. Metamorph. Geol. 34, 917–940. https://doi.org/10.1111/jmg.12214.

Wopenka, B., Pasteris, J.D., 1993. Structural characterization of kerogens to granulite-facies graphite: applicability of Raman microprobe spectroscopy. Am. Mineral. 78 (5–6), 533–557.